STUDY OF PHOTOPRODUCTION ON THE REACTION $\gamma p \rightarrow \eta p$ BY USING MONTE CARLO SIMULATION

A Dissertation

Submitted to Dean Office Institute of Science and Technology Tribhuvan University, Kirtipur in the Partial Fulfillment for the Requirement of Master's Degree of Science in Physics

By

Devshree Tripathee

December, 2017

RECOMMENDATION

It is certified that **Miss Devshree Tripathee** has carried out the dissertation work entitled **"STUDY OF PHOTOPRODUCTION ON THE REACTION γp → *ηp* BY USING MONTE CARLO SIMULATION"** under my supervision.

I recommend the dissertation for the partial fulfillment of the requirement for the degree of Master of Science in Physics at Tribhuvan University.

……..

(Supervisor)

Assoc. Prof. Kabiraj Bantawa

Tri-Chandra Campus, Ghantaghar

Kathmandu, Nepal

Date: ……..

ACKNOWLEDGEMENT

At first I would like to express my deepest gratitude to Assoc. Prof. Dr Kabiraj Banatawa, for his constant support and inspirable guidance.During my tenure,he contributed me freedom to work,engaging me in new ideas and demanding a high quality of work in all my endeavors.

I would like to thank to Asst. Prof Rajesh Mahaju (Campus Chief), Assoc. Prof. Dr. Leela Pradhan Joshi (Head of Department of Physics), Asst. Prof. Pitamber Shrestha (Co-ordinator) from Amrit Science Campus, Lainchour, Kathmandu for valuable suggestion and encouragement throughout my work. I express my sincere gratitude to all my respected teachers of Amrit Science Campus for their precious suggestion.

I am indebted to my family members father Krishna Prasad Tripathee, mother Sita Tripathee, sister Jay shree Tripathee and brother Shree Ram Tripathee for supporting me both financially and morally.

I want to thank my friends Ramesh Adhikari, Dilman Shakya, Pradeep Sagar Giri and Dinesh Koirala and staff of United Academy for constantly encouraging me directly or indirectly for my study and work.

Devshree Tripathee

December

2017

EVALUATION

We certify that we have read this dissertation entitled "STUDY OF PHOTO PRODUCTION ON THE REACTION $\gamma p \longrightarrow \eta p$ BY USING MONTE CARLO SIMULATION", and in our opinion, it is satisfactory in the scope and quality as a dissertation in the partial fulfillment for the requirement of Master's Degree of Science in Physics.

Evaluation Committee:

……	……	……
Assoc. Prof. Dr. K.R. Bantawa	Asso. Prof. L.P Joshi	Asst. Prof. Pitamber Shrestha
(Supervisor)	(HOD)	(Co-ordinator)
Tri-Chandra Campus,	Department of Physics,	Department of Physics
Kathmandu, Nepal	Amrit Campus, Lainchour	Amrit Campus, Lainchour

……	……
External Examiner	Internal Examiner

Date:

ABSTRACT

Monte Carlo simulation provides virtual experimental set up for the study of photo production reaction $\gamma p \rightarrow \eta p \rightarrow \gamma\gamma p$ in Linux based system. Within the range of threshold energy (710 MeV) for eta meson, photo production events were generated. The generated event includes generation of eta meson, proton, two photons, beam and target vertex. *dat*files were created in Linux which include the energy of gamma photon, length of target etc for the energy range $711 \leq E_\gamma \leq 1510\ MeV$. Then the *dat* files were run by using the *mkin* software which generates events. Thus the generated events were identified by using *cbsim* software. The detected events include identification of position of eta mesons, outgoing photons, proton, vertex identification, detection of position of elements in Crystal Ball (NaI) and TAPS (BaF_2) crystal and detection of energy and momentum. We found the invariant mass of eta meson and proton are 550 MeV and 938 MeV respectively according to Particle Data Group.

Keywords: Monte Carlo simulation, eta meson, proton, photons, photo production

CONTENTS

LIST OF TABLES

LIST OF FIGURES

CHAPTER 1

Introduction

1.1Elementary Particles

Elementary-particle physics deals with the fundamental constituents of matter and their interactions. In the past several decades enormous number of experimental information has been accumulated, and many patterns and systematic features have been observed. Highly successful mathematical theories of the electromagnetic, weak, and strong interactions have been devised and tested. These theories, which are collectively known as the standard model, are almost correct description of Nature, to first approximation, down to a distance scale 1/1000th the size of the atomic nucleus. There are also speculative but encouraging developments in the attempt to unify these interactions into a simple underlying framework, and even to incorporate quantum gravity in a parameter-free "theory of everything." In this article we shall attempt to highlight the ways in which information has been organized, and to sketch the outlines of the standard model and its possible extensions.

The problems concerning the *elementary particles* are today the focus of interest and of research for the experimental as well as the theoretical physicists. Experimental investigations of elementary particles involve some source of particles to study and some way of detecting those particles and measuring their behavior. Many of the practical problems of such investigations are caused by the fact that many elementary particles are unstable. The classical *elementary particle,* the individual atom was nothing but the mass point of classical mechanics. The investigation of electromagnetic phenomena suggested that *the atom* had an internal structure. At that time, the typical photo-type of elementary particle was the *electron*. The problem of the dualistic nature of matter was resolved by the quantum theory of fields: the elementary particles are nothing but the quanta of a corresponding field. The study of elementary particles is basis to the understanding of radiation phenomena, or one may regard any kind of radiation as a flux of elementary particles.

In the present work we intend to compare our results with the results obtained from previous simulation as well as experimental works using Monte Carlo simulation using mkin, cbsim software within root framework.

In 1932, when Chadwick identified the neutron and Heisenberg suggested that atomic nuclei consisted of neutrons and protons, it seemed as if proton (p), neutron (n) and electron (e^-) were sufficient to account for the structure of matter. Besides these, there was the electron exists between the nucleus and electron in the atom which plays the intermediary or field particle for the electromagnetic forces. If anti-matter exists then it would be then be made of anti-electrons, i.e. protons, anti-protons and anti-neutrons. Thus, seven particles could explain both matter and antimatter. In 1935, Yukawa postulated the existence of another particle, with the mass 200 mesa the field particle for the strong nuclear forces [1]. Recently the high-energy accelerator studies have revealed the existence of numerous new nuclear particles made partly on high-energy cosmic ray particles and other more particles. Apart from a dozen, the particles have very short lifetimes, a very much less than 10^{-8}sec. Therefore, they cannot be considered as normal constituents of matter. They are characterized by the parameters: mass, spin, electric charge and magnetic moment. The word fundamental implies that the particles are the basic building blocks of matter [1, 3].

1.2 The Classification and the Quarks

The fundamental entities that form the basis of the Standard Model are so small in size that they are treated as almost point like particles. Their sizes are most likely less than 10^{-16} m, a limit that we cannot reach at present.

Elementary particles can be categorized on the basis of spin, with the help of the quantum statistics, and may be divided into two parts:

i. Integral spin particles (follows Bose-Einstein statistics)

ii. Half integral spin particles (follows Fermi-Dirac statistics)

Spin half particles are called fermions. The modern theory of elementary particles is built on the existence of six quarks called *u* (up), *d* (down), *s* (strange), *c* (charm), *b* (bottom) and *t* (top) quark. Most peculiar property of the quarks is that these carry a fraction of charge, i.e. -1/3e (for b, d and s) and +2/3e (for u, c and t). Besides these, there are three generations of leptons associate with these quarks, called electron (e^-), muon (μ^-) and tau (τ^-) and their neutrinos.

These 12 particles (and their antiparticles) are the basic building blocks of matter. As an example, three quarks (*uud*) make a proton and three quarks (*udd*) make a neutron.

The bosons have integral spin and follow the B.E statistics. These are classified into two categories

i. Field quanta – photon, vector boson, and gluon and graviton

ii. Mesons

Some examples of mesons are,

a) Pions (π^+, π^-, π^0) **b)** Kaons (K^+, K^-, K^0) **c)** Eta (η)

Fermions are divided into two categories:

i. Light fermions or, leptons **ii.** Baryons

The light fermions consist of the six leptons. Some of the common baryons are,

a) Proton (p) and Neutron (n) **b)** Hyperons

Some examples of hyperons are,

i. Lambda (Λ^0) **ii.** Sigma ($\Sigma^+, \Sigma^-, \Sigma 0$) **iii.** Omega ($\Omega -$) and many more.

The baryons and the mesons together are also called as hadrons. All the baryons and mesons are necessarily composed of quarks.

As per the consequences of the Dirac equation, all these particles have an antiparticle with opposite charge. The symbol of these antiparticles is same as particles with a horizontal bar added above the symbol (exceptions are electron, muon and τ -lepton).

All the baryons and mesons can be constructed from these quarks. A baryon consists of three quarks whereas a meson consists of one quark and one anti-quark

As examples, we have:

Proton, $p=uud$, Neutron, $n=udd$ Kaons , $k^+ = u\bar{s}, \pi^+ = u\bar{d}$

Thus, the quarks are rightly called the basic building blocks of matter.

1.3 Fundamental interactions

Fundamental interaction or particle interactions in this case are also known as fundamental forces which are the interaction in physical systems that don't appear to be reducible to more basic interactions. There are four conventionally accepted fundamental interactions - gravitational, electromagnetic, strong nuclear and weak nuclear forces. Each one is understood as the dynamics of field.

1.3.1 Gravitational Interaction

Gravitational interaction is the weakest among other interaction, infinite range, always attractive, relative strength $10^{-40}$for sub-nuclear particle is very small (measurable for macroscopic particle only). In terms of a dimensionless constant

$$g_{m.} = \sim 6 \times 10^{-39}$$

Where $m = 1.6 \times 10^{-27}$ *kg*, which is very small so this type of interaction can be neglected into nuclear physics. The quantum of gravitational field is "graviton"; a boson having spin 2. Its characteristic time is 10^{-16} *sec*. The mass of graviton is zero, so its velocity is equal with velocity of light. As the gravitational field is very weak, the graviton cannot be detected in laboratory. The gravitational interaction does not depend upon the color, size, charge, velocities and angular orientation but depends upon the magnitude of the inertia.

1.3.2 Electromagnetic Interaction

The electromagnetic interaction is weaker than the strong interaction, but stronger than the weak and gravitational interactions. It is associated with electric and magnetic fields and is responsible for atomic structure, chemical reactions, the attractive and repulsive electromagnetic forces associated with electrically charged or magnetically polarized particles, and all other electromagnetic phenomena [1]. All of the ordinary chemical and biological effects are due to the interactions of electric charges and the fields they produce. The term electromagnetism is because the electricity and magnetism are both part of the same phenomenon. The appropriate law for the interaction of point charges bears the name of Coulomb ($F=q_1q_2/4\pi\varepsilon_0 r^2$). For two protons 10^{-15} *meter* apart, the repulsion forces will be approximately *30 Newton*. It is about 10^{35} times greater than the gravitational attraction caused by the mass. The

energy released during the complete separation of these protons will be $3\ x10^{-14}$ Joules. The inverse square law of Coulomb force may be convinced of as due to photon exchange [1, 3].

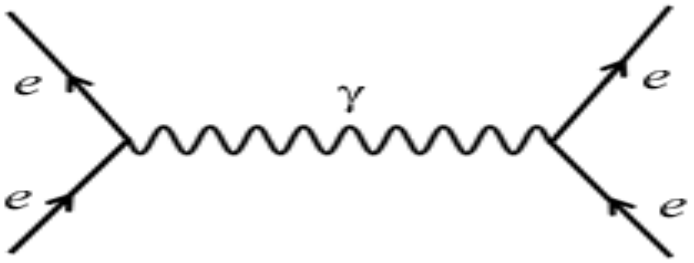

Figure 1.1: Schematic diagram of electromagnetic interaction. Photon is responsible for exchange of particle in electromagnetic interaction [3].

If the particles are not at rest but are moving, the field will not only be an electric field but would be new one depending on the velocity and magnitude of the charge. When the charge accelerated, the energy radiates out in the form of electric and magnetic pulses. This energy comes from the agent that accelerates the charge. The pulse is called a photon and travels with the velocity of light. If the source charge is accelerating in an oscillating pattern, the propagated signal will consist of successive waves of electric and magnetic fields or the radio -photon. Thus, we see that the photons are emitted and absorbed by a charge. Interaction between two charged particles consists of an exchange of these photons. The strength of the electromagnetic interaction is given by the dimensionless fine structure constant ($\alpha = e^2/\varepsilon_0\hbar c = 1/137$), and is due to photon exchanges. [3]

The capture of photon can affect the production of mesons and hyperons by name interaction

$$\gamma + p \longrightarrow \pi^0 + p,$$

$$\gamma + p \longrightarrow \Lambda^0 + K^+.$$

An example of radioactive capture reaction is

$$\pi^- + p \longrightarrow n + \gamma.$$

The neutral particles such as

$$\pi^0 \longrightarrow \gamma + \gamma,$$

$$\Sigma^0 \longrightarrow \Lambda^0 + \gamma,$$

$$\eta^0 \longrightarrow \pi^+ + \pi^- + \pi^0,$$

$$\eta \longrightarrow \gamma + \gamma$$

Decay electromagnetically since these processes involve no change of strangeness. The decay processes such as $\Sigma^+ \rightarrow p^+ + \gamma$ are forbidden because the change $\Delta S = 1$ is required. The paradox that the decay of neutral particle is resolved by introducing as intermediate step in all overall reaction the virtual production of a nucleon , anti - nucleon, (or electron -positron) pair. Thus, we have

$$\pi \longrightarrow (N + N) \longrightarrow \gamma + \gamma.$$

The process of mutual annihilation of particles and anti-particles is an example of electro-magnetic interaction [1, 5].

1.3.3 Strong Interaction

Strong interaction is interaction between elementary particles responsible for the forces between nucleons in the atomic nucleus. It operates at distances less than about 10^{-15}meters, and is about a hundred times more powerful than the electromagnetic interaction [3]. This type of interaction is always attractive and suitable to explain the existence of stable nuclei. Strong interaction is responsible for most nuclear phenomenon, nuclear energy level. Its relative strength is approximately 1 and is independent of electric charge i.e. p-p, p-n, n-n interaction. Strong interaction does not obey inverse law [4]. Here the

Coupling constant $= g^2 / 4\pi hc,$ where g = pions- nucleon coupling constant.

Strong interaction force is of nuclear origin and is strong enough to overcome the repulsive force between densely packed protons in the nucleons. Strong interaction between hadrons should be traceable to an interaction between quarks. The particles that exchange the quarks to produce this interaction are called “gluons”. Strong interaction falls off rapidly when the distance between two particles increases. For example, interaction is generated by exchange of single pions. Strong interaction between two elementary particles is responsible for the cross section as a function of

energy. Strong interaction is responsible for kaons production; however the decay of mesons, nucleons and hyperons proceeds by an electromagnetic or weak interactions [1].

1.3.4 Weak interaction

Weak interaction is an interaction between elementary particles that is responsible decay processes, operates at distances less than about 10^{-15} meters, and is 10^{12} times weaker than the strong interaction [3].The weak interaction and electromagnetic interactions are, now, described by the unifying electro-weak theory. The weak interaction is responsible for the decay of strange and non -strange particles and for non-leptonic decays of strange particles. The numerical constant, which is characteristics of the weak interactions, is obtained from Fermi's theory of beta decay [4]**.** This type of interaction is applicable to hadrons & leptons, neutrino & antineutrino. Weak interaction is responsible for the radioactive beta decay of subatomic particle & initiates the process known as hydrogen fusion in stars. This type of interaction affects all fermions ($s = 1/2$). Most noticeable example when particle undergoes beta decay, deuterium and helium are produced from hydrogen. Coupling constant is given by Fermi's theory $= (gF/(\hbar c)^2)/(m_\pi c/h) \sim 5 \times 10^{-14}$ In 1968, the electromagnetic force and the weak interaction were unified when they were shown to be two aspects of a single force, now termed the electro weak force. The theory of the weak interaction can be called "Quantum Flavor dynamics (QFD)", in analogy with the term QCD and QED, but in practice the term is rarely used because the weak force is best understood in terms of electro - weak theory (EWT) [1, 2].

1.4. The Quark Model

Murray Gell-Mann and G. Zweig proposed the quark model in 1964 [6]. This theory is based in on the idea that the hadrons are built up from a limited number of "fundamental" units, which have acquired the name quarks [7]. The original three quarks were labeled *u* (for up), *d* (for down) and *s* (for strange). Each quark has an anti-quark associated with it ($\bar{u}$, $\bar{d}$ and $\bar{s}$). The magnitude of each of the quantum numbers for the anti-quarks has the same magnitude as those for the quarks, but the sign is changed [2]. Any of a set of six hypothetical elementary particles together with their antiparticles thought to be fundamental units of all baryons and mesons but

unable to exist in isolation. The magnitude of their charge is either two thirds or one third of that of the electron. Isolated quarks and anti-quarks have never been detected, a fact explained by confinement of spin. Every quark carries one of three color-charges of the strong interaction; anti-quarks similarly carry anti-color. Color-charged particles may combine to form color neutral composite particles called hadrons. A quark may pair up with an anti-quark: the quark has a color and the anti-quark has the corresponding anti-color. The color and anti-color cancel out, forming a color neutral meson. Alternatively, three quarks can exist together, one quark being "red", another "blue", and "green". These three colored quarks together form a color-neutral baryon. Symmetrically, three anti-quarks with the colors "anti-red", "anti-blue" and "anti-green" can form a color-neutral anti-baryon [4].

Quarks also carry fractional electric charges but they are confined within hadrons whose charges are all integral charges. So quarks have never been isolated. Each quark has spin *(-1/2*) and baryon no *(1/3).* Quarks are categorized into three types as

i. up (u) **ii**. down (d) and **iii.** strange (s)

The Unified Field Theory (UFT) of physics was developed to explain the basic structure of hadrons. It is supposed that the hadrons are composed of two units, the quarks and gluons. The quarks are fermions with spin*1/2 ħ* and non- zero mass but gluons are bosons with spin *1ħ* (integral spin) and mass zero. The elementary particles are supposed to be built up by the combination of the quarks. The quarks *(a, b, c)* are the basic states which are represented as the basic three component column matrix.

$$a = \begin{pmatrix} 1 \\ 0 \\ 0 \end{pmatrix}, \quad b = \begin{pmatrix} 0 \\ 1 \\ 0 \end{pmatrix}, \text{ and } c = \begin{pmatrix} 0 \\ 0 \\ 1 \end{pmatrix}$$

Where a and b form doublet spin and c form a singlet spin and corresponding anti-quarks are

$$\overline{a} = (1, 0, 0) \qquad \overline{b} = (0, 1, 0) \qquad \text{and} \qquad \overline{c} = (0, 0, 1)$$

Quarks are classified in terms of their color and flavor. Colors are red *(r),* green *(g)* and Blue (*b*) and by flavor are denoted by *u, d, s, c, t and b*. Where, *u= up, d= down, s= strange, c= charm, t= top, b= bottom.* The colored quarks were discovered to support Pauli Exclusion Principle in the case of particles like Ω^- *hyperon*. Last three quarks were discovered by Glash−ow, Iliopoulish and Mainani. The charmed quark

was suggested to explain the suppression of certain decay processes that are not observed [3].

Table 1.1: Quantum number of quarks [3, 8].

Quantum no. Flavor of quarks		Baryon no*(B)*	Spin *(T)*	Iso-spin *(Tz)*	Charge *(q)*	Strengths *(s)*	Charm *(s)*	Anti-Quarks
u	Up	*1/3*	½	*1/2*	*2/3e*			$\overline{u}$
d	Down	*1/3*	½	*-1/2*	*-1/3e*			$\overline{d}$
s	Strange	*1/3*	½		*-1/3e*	*-1*		$\overline{s}$
c	Charm	*1/3*	½		*2/3e*		*1*	$\overline{c}$
t	Top	*1/3*	½	*1/2*	*2/3e*			$\overline{t}$
b	Bottom	*1/3*	½	*1/2*	*-1/3e*			$\overline{b}$

There are *18* quarks and *18* anti-quarks. The top and bottom quarks are not as usual. The non- strange mesons *(s=0)* consists of one quark and one anti-quark or a superposition of these quarks. The spin could be zero or *1* [2].

1.5 Composition of hadron according to quark model

Hadron is a composite particle made of quarks held together by the strong force (just like molecules are held together by the electromagnetic force). Hadron may be baryons or mesons. A baryon is made up of three quarks and meson is made up of one anti quark. For example, protons are made of two quarks *u* and *d* quarks (*uud*). For these quarks, the electric charges are *+2/3 , +2/3 and -1/3* , for a total value of *+1*. The baryon number is *+1/3, +1/3 and +1/3* for a total of *+1*. The strangeness number is *0, 0*, and *0* for a total strangeness of *0*. All are in agreement with the quantum numbers for the proton.

Mesons are made up of one quark and one anti-quark. For example, the pions are an example of a mesons, the π is the combination of a *u* quarks and a *d* anti-quark $(u\bar{d})$.Electric charges of these quarks are *+2/3* and +1/3 for a total of *+1*. The baryon numbers are *+1/3* and *-1/3* for a total baryon number of zero. The strangeness numbers are *0* and *0* for a total of *0*. All of these are in agreement with the quantum number for the π^- mesons. Quarks all have spins of *1/2*, which accounts for the observed half-integral spins of baryons, *0* and *1* spins of mesons.

All known hadrons can be explained in terms of the various quarks and their anti-quarks. Table 1.1 shows the quarks contents of six hadrons and how they amount for the observed charges, spins and strangeness numbers of these particles. For the example the quark combination of proton and neutron are shown in figure 1.2.

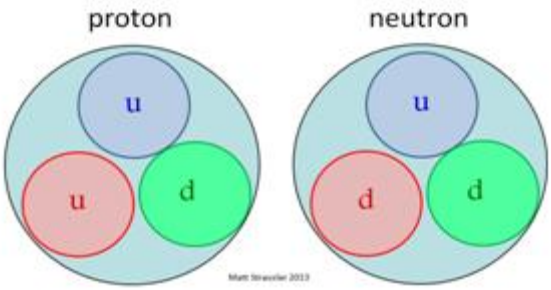

Figure 1.2: Quark combinations of proton and neutron respectively [2]

1.6 Colored Quarks and Gluons

The field that binds the quarks is a color field. Color charge is the property of quarks and gluons that is related to the particle's strong interaction same as electric charge is to the electromagnetic interaction between electrons. It is the fundamental strong charge and is carried out by the gluons.

There were problems with the quark model, one of them, was Ω^- hyperons. It was believed to contain three identical s quarks *(sss).*This violates Pauli Exclusion Principle that prohibits two or more fermions from occupying identical quantum states. The proton, neutron and others with two identical quarks would violate this principle also. We can resolve this difficulty by assigning a new property to the quarks. We can regard this new property as an additional quantum number that can be used to label the three otherwise identical quarks in the Ω^- [9]. If this additional quantum number can take any of three possible values, we restore the Pauli Exclusion Principle by giving each quark a different value of this new quantum number, which is known as color. The three colors are labeled as Red *(r),* Blue *(b)* and Green *(g).* The Ω^- for example, would then S_r, S_b, S_g. The anti-quarks colors are anti-red ($\bar{r}$), anti-blue ($\bar{b}$) and anti -green ($\bar{g}$) [8].

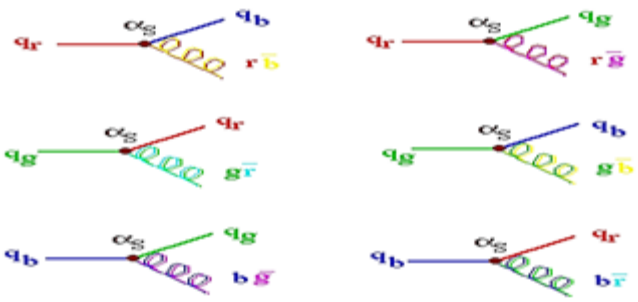

Figure 1.3: Various types of gluons [4].

An essential component of the quark model with colors is that all observed mesons and baryons states are "colorless", i.e. either color anti-color combinations in the case of mesons, or equal mixtures of *r* , *b* and *g*in the case of baryons.

Since hadrons seem to be composed of quarks, the strong interaction between hadrons should ultimately be traceable to an interaction between quarks. The force between quarks can be modeled as an exchange force, mediated by the exchange of mass less particles with spin -1 called gluons. Eight gluons have been postulated. The gluons must therefore be represented as combination of a color and possibly a different anti-color. The gluons are mass less and carry their color anti-color properties just as other particle may carry electric charge. In effect, the red quark emits its redness into a gluon and acquires blueness by also emitting anti-blueness. On the other hand, the blue quarks absorb the *RB* gluon, cancelling its blueness and acquiring a red color in the process [3].

1.7 Charm, Bottom and Top

In 1970, Glasgow, Iliopoulos, and Mariana proposed the existence of a fourth quark called *c* or charmed quark. The charm quark or *c* quark (from its symbol, *c*) is the third most massive of all quarks, a type of elementary particle. Charm quarks are found in hadrons, which are subatomic particles made of quarks. The first charmed particle (a particle containing a charm quark) to be discovered was the *J/ψ* meson. A team at the Stanford Linear Accelerator Centre (SLAC) discovered it [9]. The charmed quarks were suggested to explain the suppression of certain decay process that is not observed. With only three quarks, the process would proceed at measurable rates and should have been observed. The charm quark has a charge *2/3e*, strangeness *0* and a charm quantum number of *+1*, other quarks have *0* charms [3].

In 1977, a new particle was discovered at Fermi Lab that provides evidence for yet another quark. This particle, called the upsilon-meson, was thought to be made up of the new quark called *b* (for bottom or beauty) along with the associated anti -quark with electric charge *-1/3e.*Because quarks seem to come in pairs, it is expected that there is a partner to the quark, called *t* (for top). It has charge of *+2/3e* [1].

1.8 Three Generations of quarks and leptons

Both leptons and quarks appear to come in three generations of doublets, with all particles having spin *1/2*. The first generation contains two leptons: the electron and electron neutrino, and two quarks, up and down. All the properties of ordinary matter can be understood on the basis of these particles. The second generation includes the muon and muon neutrino and the charm and strange quarks. These particles are responsible for most of unstable particles and resonances created in high-energy collisions. The third generation includes the tau and tau neutrino and the top and bottom quarks [3].

The table 1.2 shows the properties of the three generation of quarks in terms of charge, isospin, spin, strange, charm bottom, top number and their respective mass.

Table 1.2: Properties of the Three Generations of Quarks [3, 8].

Generation	*Name*	*Symbol*	*Charge (Q)*	*Isospin (I_3)*	*Spin*	*S*	*C*	*B*	*T*	*Mass GeV/C^2*
1	*Down*	*d*	*-1/3*	*-1/2*	*1/2*	*0*	*0*	*0*	*0*	*0.35*
	Up	*u*	*+2/3*	*+1/2*	*1/2*	*0*	*0*	*0*	*0*	*0.35*
2	*Strange*	*s*	*-1/3*	*0*	*1/2*	*-1*	*0*	*0*	*0*	*0.5*
	Charm	*c*	*+2/3*	*0*	*1/2*	*0*	*1*	*0*	*0*	*1.5*
3	*Bottom*	*b*	*-1/3*	*0*	*1/2*	*0*	*0*	*-1*	*0*	*4.5*
	Top	*t*	*+2/3*	*0*	*1/2*	*0*	*0*	*0*	*1*	*171*

Table 1.3: Properties of the three Generations of Leptons [3].

Generation	*Lepton*	*Symbol*	*Charge*
1	*Electron*	e^-	*-1*
	e-neutrino	ν_e	*0*
2	*Muon*	μ^-	*-1*
	μ *– neutrino*	ν_μ	*0*
3	*Tau*	τ^-	*-1*
	τ *–neutrino*	ν_τ	*0*

1.9 Mesons in the quark model

Mesons are bound states of a quark and an anti-quark with zero baryon number. Mesons can be placed in the singlet and octet representations. Since quarks are spin-*1/2* fermions, in a meson $q\overline{q}$ pair must have a total intrinsic spin equal to *0* or *1*. The parity of a meson is expressed as $(-1)^{L+1}$

Some examples of mesons are as follows.

Table 1.4: Mesons properties [8, 9]

Particle	*Symbol*	*Anti-particle*	*quark content*	*Rest Mass MeV/c²*	*S*	*C*	*B*	*Life time*	*Decay Modes*
Pion	π^+	π^-	$u\overline{u}$	*139.6*	*0*	*0*	*0*	2.60×10^{-8}	$\mu^+\nu_\mu$
	π^0	*Self*	*ud*	*135.0*	*0*	*0*	*0*	0.83×10^{-16}	2γ
Kaon	K^+	K^-	*us*	*493.7*	*+1*	*0*	*0*	1.24×10^{-8}	$\mu^+\nu_\mu$, $\pi^+\pi^0$
	K^0_s	K^0_s		*497.7*	*+1*	*0*	*0*	0.89×10^{-10}	$\pi^+\pi^-, 2\pi^0$
	K^0_L	K^0_L		*497.7*	*+1*	*0*	*0*	5.2×10^{-8}	$\pi^+ e^- \nu_e$
Eta	η^0	*Self*	$u\overline{u}$, $d\overline{d}$	*548.8*	*0*	*0*	*0*	$<10^{-18}$	2γ, 3μ
Rho	ρ^+	ρ^-	*u d*	*770*	*0*	*0*	*0*	0.4×10^{-23}	$\pi^+\pi^0$
	ρ^0	*Self*	*u, d*	*770*	*0*	*0*	*0*	0.4×10^{-23}	$\pi^+\pi^-$
Omega	ω^0	*Self*	*u, d*	*782*	*0*	*0*	*0*	0.8×10^{-22}	$\pi^+\pi^-\pi^0$
Phi	Φ	*Self*	*S*	*1020*	*0*	*0*	*0*	20×10^{-23}	K^+K^-, K^0K^0

Where, *L* is the orbital angular momentum of the q pair. In the ground state (*L= 0*) a meson always has negative parity. Mesons with total spin zero and odd parity $(J^P = 0)$

are called pseudo scalar mesons. The nine members of the octet and singlet form a pseudo scalar meson nonet. The lightest pseudo scalar mesons include pions *(π)* with strangeness 0 and kaons (*K*) with strangeness *+1*. Likewise, the mesons with spin one and odd parity ($J^P = 1$) are called vector mesons, and the nine members of the vector-meson octet and singlet form a vector-meson nonet [3].

1.10 Baryons in the quark model

Baryons are bound states of three quarks with baryon number one. Each baryon has a corresponding antiparticle called an anti-baryon in which the quarks are replaced by their corresponding antiquarks. Baryons can be placed in the singlet, octet, and decuple (tenfold) representations. Some examples of baryons are as follows

Table 1.5: Baryons properties [3].

Particle	*Symbol*	*quark content*	*Rest mass (MeV/c^2)*	*Spin*	*B*	*S*	*Lifetime (seconds)*	*Decay Modes*
Proton	P	uud	938.3	1/2	+1	0	Stable	...
Neutron	N	udd	939.6	1/2	+1	0	920	$p\ e^-\ \nu_e$
Lambda	Λ^0	$u\bar{d}s$	1115.6	1/2	+1	-1	2.6×10^{-10}	$p\ \pi^-,\ n\ \pi^0$
Sigma	Σ^+	$u\bar{u}s$	1189.4	1/2	+1	-1	0.8×10^{-10}	$p\pi^0,\ n\ \pi^+$
	Σ^0	uds	1192.5	1/2	+1	-1	6×10^{-20}	$\Lambda^0\gamma$
	Σ^-	uds	1197.3	1/2	+1	-1	1.5×10^{-10}	$n\ \pi^-$
Delta	Δ^{++}	$u\bar{u}u$	1232	3/2	+1	0	0.6×10^{-23}	$p\ \pi^+$
	Δ^+	$u\bar{u}d$	1232	3/2	+1	0	0.6×10^{-23}	$p\pi^0$
	Δ^0	$ud\bar{d}$	1232	3/2	+1	0	0.6×10^{-23}	$n\pi^0$
	Δ^-	$d\bar{d}d$	1232	3/2	+1	0	0.6×10^{-23}	$n\ \pi^-$
Xi	Ξ^0	$us\bar{s}$	1315	1/2	+1	-2	2.9×10^{-10}	$\Lambda^0\pi^0$
	Ξ^-	$ds\bar{s}$	1321	1/2	+1	-2	1.64×10^{-10}	$\Lambda^0\pi^-$
Omega	Ω^-	$s\bar{s}s$	1672	3/2	+1	-3	0.82×10^{-10}	$\Xi^0\pi^-,\ \Lambda^0K^-$
Lambda	Λ^+_c	uds	2281	1/2	+1	0	2×10^{-13}	...

The most common baryons are the proton and neutron: $p = |uud\rangle$ *and* $n = |udd\rangle$ which are collectively called nucleons *(N)*. The baryon octet with $J^P = (1/2)^+$ also includes the iso-singlet Λ and iso-triplet Σ baryons with strangeness -1. Baryons with non-zero strangeness are called hyperons. The Λ *(uds)* with $B = 1,\ Q = 0,$ *and* $S = -1$ is the lightest hyperon or strange baryon. Every baryons has antiparticle called anti-baryons having baryons number (-1) [3].

1.11 Particles code

Internally GEANT uses different codes for different particles some of them are shown in the table below

Table 1.6: Particle codes [10].

GEANT Code	Particle	GEANT Code	Particle	GEANT Code	Particle
1	Γ	*16*	K^0_S	*31*	$\bar{\Xi}^+$
2	e^+	*17*	H	*32*	$\bar{\Omega}^+$
3	e^-	*18*	Λ	*33*	τ^+
4	Y	*19*	Σ^+	*34*	τ^-
5	μ^+	*20*	Σ^0	*35*	D^+
6	μ^-	*21*	Σ^-	*36*	$\bar{D}$
7	π^0	*22*	Ξ^0	*37*	D^0
8	π^+	*23*	Ξ^-	*38*	$\bar{\mathrm{D}}^0$
9	$\bar{\pi}$	*24*	Ω	*39*	D_s^+
10	K^0	*25*	$\bar{n}$	*40*	$\bar{\mathrm{D}}_\mathrm{s}^-$
11	K^+	*26*	$\bar{\Lambda}$	*41*	Λ_c^+
12	K^-	*27*	$\bar{\Sigma}^-$	*42*	W^+
13	N	*28*	$\bar{\Sigma}^0$	*43*	W^-
14	P	*29*	$\bar{\Sigma}^+$	*44*	Z^0
15	$\bar{\mathrm{p}}$	*30*	$\bar{\Xi}^0$		

CHAPTER 2

Kinematics of eta meson photoproduction

The eta (η) meson made of a mixture of *up*, *down* and *strange quarks* and their *anti-quarks*. The η is a pseudo scalar meson.

2.1 Properties of η meson

Table 2.1: Properties of eta meson

Property	Value
Mass	$(547.51\pm 0.18)\ MeV/c^2$
Valence Quarks	$(u\bar{u} + d\bar{d} - 2s\bar{s})/\sqrt{6}$
Life Time	$<10^{-18}\ sec$
Charge (Q)	*0*
Iso-spin (I)	*0*
Orbital Angular Momentum(L)	*0*
Total Angular Momentum (J)	*0*
Strangeness (S)	*0*
Parity (P)	-
Charge Conjugation (C)	+
Interaction	*Strong, Weak , Gravitational*
Antiparticle	*Self*

2.2 Decay mode

The proton can be made excited using photons with energies $E_{th} \geq 711.35MeV$ producing the reaction

$$\gamma p \rightarrow \eta p \qquad (2.1)$$

Eta meson is a particle having life time of $< 10^{-18}$sec, decay before detection of the various decays of the eta 72 % occur via the following neutral modes.

$$\eta \rightarrow 2\gamma, \qquad (2.2)$$

$$\eta \rightarrow 3\pi^0 \rightarrow 6\gamma \qquad (2.3)$$

with branching ratio of *(39.39 ± 0.24) %* and *(32.52 ± 0.26) %* respectively [8]. The main aim of this thesis work is to study photo production reaction $\gamma p \rightarrow \eta p \rightarrow \gamma\gamma p$.

2.3 Kinematics for $\gamma p \rightarrow \eta p$

In our experiment, liquid hydrogen was used as the target. After the interaction of the incident photon beam with the proton, the outgoing η makes a polar angle θ with respect to the direction of the incident photon.

Let us consider P^{μ}_{beam} , P^{μ}_{target} , P^{μ}_{η} and P^{μ}_{p} are the four - momenta of the incident photon, target proton, η meson and product proton respectively. Now, using the energy-momentum conservation relation in four -momenta notation, we may write

$$P^{\mu}_{beam} + P^{\mu}_{target} = P^{\mu}_{\eta} + P^{\mu}_{p} \qquad (2.4)$$

The superscript letter μ takes four value $\mu = 0, 1, 2, 3$ where μ = 0 gives the energy (*E*) and other values of μ represent the three –momenta $(P = P^1, P^2, P^3)$ of the four vector (P^{μ}). The four momenta of η is determined by summing the four momenta of its photon decays (2γ) as

$$P^{\mu}_{\eta} = \sum_{i=1}^{2} P_{\gamma i}^{\mu} \qquad (2.5)$$

In the laboratory frame, these four momenta can be expressed as

$$P^{\mu}_{beam} = (E_{beam}, P_{beam}) \qquad (2.6a)$$

$$P^{\mu}_{target} = (E_{target}, P_{target}) = (M_{target}, 0) \qquad (2.6b)$$

$$P^{\mu}_{\eta} = (E_{\eta}, P_{\eta}) \qquad (2.6c)$$

Since the square of the target four momenta gives the invariant mass of the target (M_{target}), we can write

$$P^2_{target} = P^{\mu}_{target} . P_{\mu target} = E^2_{target} - P^2_{target} = M^2_{target} \qquad (2.7)$$

As the target is at rest in the laboratory frame, it follows that $P_{target} = 0$ and $E_{target} = M_{target}$. The photon energy $E_{beam}$is measured by using the Virtual Photon Tagger and $E_{beam} = P_{beam}$in equation *(2.6a)*. When there is only one undetected particle in the final state like proton here, its kinematics is reconstructed by using four-momentum

conservation [11]. Using Equations *(2.4.)* and *(2.6c)*, the four momenta $P^{\mu}{}_{p}$of the undetected proton can be expressed as

$$P^{\mu}{}_{p} = P^{\mu}{}_{beam} + P^{\mu}{}_{target} - P^{\mu}{}_{\eta}$$

$$P^{\mu}{}_{p} = P^{\mu}{}_{beam} + P^{\mu}{}_{target} - \sum_{i}{}^{2} P_{\gamma i}{}^{\mu} \qquad \textit{(from 2.5)} \qquad (2.8a)$$

Using equation (2.6a) and (2.6b)

$$E_{p} = E_{beam} + M_{target} - E_{\gamma} \qquad (\mu=0) \quad (2.8b)$$

$$P_{p} = P_{beam} \qquad (\mu=1) \quad (2.8c)$$

Thus the missing mass *MM (η)* of the *η* is given as

$$MM\ (\eta) = M_{p} = \sqrt{(E_{p}{}^{2} - P_{p}{}^{2})} \qquad (2.9)$$

The outgoing η makes a polar angle θ with respect to the direction of the incident photon [8].

2.3.1 Event Selection

The eta meson has a very short lifetime, so only the photons resulting from their decay are determined by $\eta \rightarrow 2\gamma$. When a particle decays, its four momenta vector is conserved. Consequently, the four-vector momenta of an eta meson are equal to the sum of the momenta four-vector of the photons resulting from its decay. For our research work of $\gamma p \rightarrow \eta p \rightarrow 2\gamma p$, two photons and a proton are in the final state [11].

2.3.2 Particle Identification in $\gamma p \rightarrow \eta p \rightarrow 2\gamma p$

As we have seen, the final state, we detected that two photons and a proton. As we know that lifetime of η mesons is very short, so only the photons resulting from their decays $\eta \rightarrow 2\gamma$ were detected. The four-vector momenta of η events were identified by constructing the invariant mass of the two photons.

For the reaction $\gamma p \rightarrow \eta p \rightarrow 2\gamma p$, *all* information about the initial state was available: the energy of the incident photon beam and its direction (along the beam axis), and the target nucleon, which was assumed to be at rest. The four-vector momenta vector of the η (the four-vector of the two decay photons) was also known. Thus using the

principle of conservation of energy and momentum, the four -vector of missing particle i.e. eta is given by

$$P^{\mu}_{\eta} = P^{\mu}_{beam} + P^{\mu}_{target} - \sum_i^2 P_{\gamma i}^{\mu} \quad (2.10)$$

Where, P_{beam} and P_{target} are the corresponding momentum four-vectors of the incident photon and target nucleon, respectively. For the target nucleon, we assumed $P_{target} = (M_p , 0)$, where M_p is the proton mass [8, 11]

2.3.3 Identification of a proton by missing mass

In the reaction $\gamma p \rightarrow \eta p \rightarrow 2\gamma p,$ the proton is an undetected particle; however, it can be reconstructed. As the momentum four-vectors of the incoming photon beam, the target proton and the two final states photon are known, the four momentum of the missing

$$P^{\mu}_{proton} = P^{\mu}_{beam} + P^{\mu}_{target} - \sum_i^2 P_{\gamma i}^{\mu} \quad (2.11)$$

The missing mass-squared of the two photons in the final state ($MM_{2\gamma}$) is obtained by squiring the four-vector P_{proton} as

$$(MM_{2\gamma})^2 = (P_{proton})^2 \quad (2.12)$$

So missing mass of two photon provides proton mass. [12]

2.4 Threshold Energy Expression

The minimum energy of photon required to produce eta meson is called threshold energy of eta meson. Consider a beam of photon strikes liquid hydrogen target at rest and product particles are eta meson and photon. So our reaction becomes

$$\gamma p \rightarrow \eta p$$

Then from law of conservation of momentum, initial momentum of the reactant is equal to the final momentum of the product. So we can write

$$(P^{\mu}_{beam} + P^{\mu}_{target})^2 = (P^{\mu}_{\eta} + \sum_i^2 P_{\gamma i}^{\mu})^2 \quad (2.13)$$

Where P^{μ}_{beam} , P^{μ}_{target} , P^{μ}_{η} , $\sum_i^2 P_{\gamma i}^{\mu}$ are the four momentum of the incident photon, target proton, η meson and product proton respectively.

So, $(E_\gamma + E_p)^2 - (P_\gamma + P_p)^2 = (E_\eta + E_p)^2 - (P_\eta + P_p)^2$ (2.14)

Since m the four momenta of eta and proton, which is zero .i.e.P_η , $P_p = 0$, $E_p = m_p$ and $E_\eta = m_\eta$

$$E^2_\gamma + 2E_\gamma m_p + m^2_p - P^2_\gamma = m^2_\eta + m_p{}^2 + 2m_p m_\eta \quad (2.15)$$

$$E^2_\gamma - P^2_\gamma + 2E_\gamma m_p = m^2_\eta + 2m_p m_\eta \quad (2.16)$$

$E^2_\gamma - P^2_\gamma = 0$, because real photon has no mass and its momentum and energy are same [9]

This gives threshold energy for the reaction $\gamma p \rightarrow \eta p$

$$(E_\gamma)_{threshold} = (m^2_\eta + 2m_p m_\eta) / 2m_p \quad (2.17)$$

For the reaction $\gamma p \rightarrow \eta p$,

$m_\eta = 550.095\ MeV$

$m_p = 938.27\ MeV$

Then equation (2.17) gives

$$E_{\gamma\ threshold} = 711.35\ MeV$$

This is the minimum energy of photon beam required to produce η meson. Therefore for the reaction $\gamma p \rightarrow \eta p$, we have to provide energy of photon more than threshold energy. For this purpose, we prepare different data file (*'dat file'*) with energy of incident photon more than threshold energy [11].

CHAPTER 3

Review of photoproduction $\gamma p \rightarrow \eta p$

Over the last several years, there has been increasing number of work in the photoproduction of eta mesons with protons. One of the first eta meson nuclear experiments performed at SATURNE in 1988 [11].

Over the last two years eta production from the nucleon has been measured at Mainz and Bonn with an accuracy of more than an order of magnitude better than in older experiments. At Mainz, the TAPS collaboration has obtained high quality data for angular distributions and total cross sections for photon energies between threshold and *790 MeV* both on the nucleon and on nuclear targets ^{12}C ,^{40}Ca which can be considered to be a qualitative breakthrough in the experimental field [11]. In this work, we have presented a study of photoproduction of eta meson i.e.

$$\gamma p \rightarrow S_{11}(1535) \rightarrow \eta p$$

As MAMI (Mainz Microtron) is helpful for the determination of tagging efficiency, nuclear cross section, further study of production process and the final state interaction without being obscured by the details of the nuclear transition densities. William A. McNeely carried out eta photoproduction with hydrogen target, at *0°* and *180°* for the energy between *0.7* and *1.1 GeV*in 1971 [15]. Similarly, *Eta (547)* and *Eta (958)* meson photoproduction on the proton was carried out by Michael Dugger in 2001[16]. In the same way measurement of the branching ratio for eta-meson decay into neutral pion and two photons, was carried out by Jason William Brudvikin 2007[14]. Eilidh Fiona McNicoll did later photoproduction study with the upgraded Glashgow tagger at MAMI from University of Glashgow, Scotland on January 2001[11]. The next two sub -sections describe these studies.

3.1 Work and result carried out by Jason William Brudvik

This dissertation presents the results of a measurement of the branching ratio for the rare decay $\eta \rightarrow \pi^{\circ}\gamma\gamma$. The experiment was carried out in the A2 hall of the Mainz Microtron facility at the Institut für Kernphysik, on the campus of Johannes Gutenberg Universität, in Mainz, Germany. The experiment used the Glashgow Mainz Tagger, which is a recoil-electron spectrometer, to determine the energy of the

incident photons. The principle detector is the Crystal Ball which is a highly segmented multi-photon spectrometer surrounding the experimental target. There is also a forward detector, TAPS, which is a multi-photon spectrometer arranged as a downstream wall of detectors. Furthermore, setup included an instrument used to differentiate between charged and neutral particles called the Particle Identification Detector, and a liquid hydrogen target. The kinematics technique was used to select the $\eta \rightarrow \pi^{\circ}\gamma\ \gamma$ events. The major backgrounds, namely $\eta \rightarrow 3\pi^{\circ}$ and decay $\eta \rightarrow \gamma\gamma$ and $2\pi^{\circ}$ production were measured simultaneously. The result for the branching ratio is BR $(\eta \rightarrow \pi^{\circ}\gamma\gamma) = (2.0 \pm 0.7) * 10^{-4}$. However, we simply study photoproduction of eta meson [19].

We used some histograms by using Monte Carlo methods. This shows invariant mass spectrum of η for $\eta \rightarrow 2\gamma$ and $\eta \rightarrow 6\gamma$ decay. The peak value of mass invariant curve is approximately $547\ MeV/c^2$ which is the mass of eta meson.

3.2 Work and Result carried out by Eilidh Fiona McNicoll

Mc Nicoll presented differential cross-section measurements for η photoproduction on the proton $\gamma p \rightarrow \eta p$, in the energy range $711 \leq E_{\gamma} \leq 1403\ MeV$ over the full polar angular range, $0^{\circ} \leq \theta_{\eta} \leq 180^{\circ}$. The two dominant $\eta\eta$ decay channels: $\eta \rightarrow 2\gamma$ and $\eta \rightarrow 3\pi^0 \rightarrow 6\gamma$ had been analyzed separately. A comparison of results from these final states was given [11].

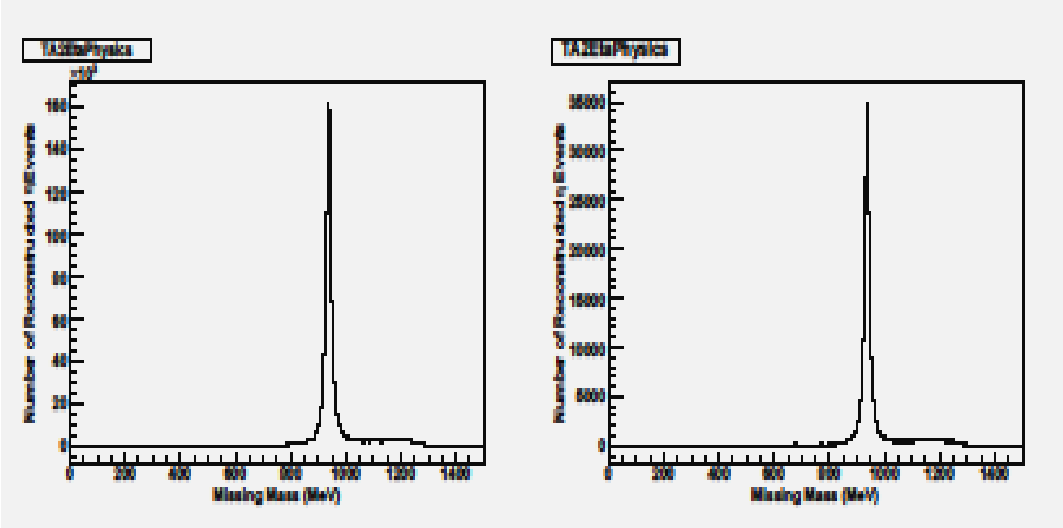

Figure 3.1: Missing mass of proton obtained from $\gamma p \rightarrow \eta p$ photoproduction analysis for $\eta \rightarrow 2\gamma$ (left) and $\eta \rightarrow 6\gamma$ (right) Study with the Upgraded Glasgow Tagger at

MAMI by Eilidh Fiona McNicoll, University of Glasgow Scotland and January, 2010 [11].

From the η photoproduction threshold at *711 MeV to 890 MeV*, the angular distribution of the differential cross-section is quite flat, indicating the dominance of s-wave processes in the reaction mechanism, in this case the $S_{11}(1535)$. The resonant shape is truncated at threshold and rises to a maximum at $E_\gamma = 805$ *MeV*, corresponding to the centre -of-mass energy of *1535 MeV*. This accounts for the cross section rise to maximum. By *1050 MeV*, this maximum has become more pronounced and moved to a forward angle [11].

Measurement of the cross section of our photo-production reaction $\gamma p \rightarrow \eta p$, is beyond scope of this work as we are not analyzing for the real data.

CHAPTER 4

Geometry of Virtual Apparatus

This chapter describes the experimental facility used by the*A2 Collaboration in Mainz,Germany.* The setset-up is mainly comprised of the three components shownin Fig.4.1.The primary component is the electron accelerator, which is also called the Mainz *Microtron (MAMI-C).* It produces a continuous-wave electron beam. The beam *MAMI-C* is directed onto a thin diamond or copper foil generating a beam of high-energy photons via a bremsstrahlung process.The second component is the *Glasgow Photon Tagging Spectrometer*, which is used to analyze the momentum of bremsstrahlung electrons.The photon beam is allowed to impinge on a target causing the production of various particles. The third component, which is the detector system used to detect these particles and their decays, consists of the *Crystal Ball (CB) and the TAPS spectrometer.*

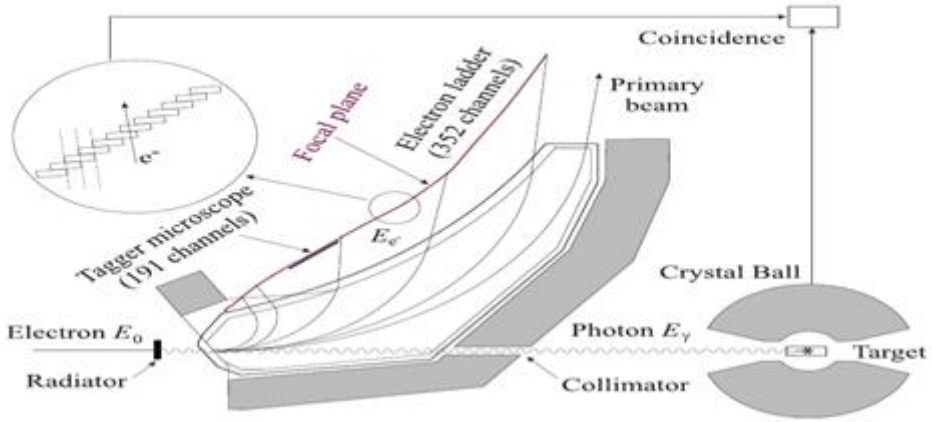

Figure 4.1: The top view of the tagger for producing Bremsstrahlung photons and experimental detector (Crystal Ball) [16].

4.1 Mainz Microtron (MAMI)

The *Mainz Microtron (MAM*I) is an intense, stable and continuous-wave accelerator that accelerates electrons to the relativistic limit. It is operated by the Institute f¨ur Kernphysik at Johannes *Guttenberg University at in Mainz, Germany*. The accelerator in its current configuration was constructed in four stages: (i) *MAMIA1,(ii) MAMI-A2, (iii) MAMI-B, and (iv) MAMI-C. MAMI-A1* was installed in 1979,producing electrons up to 14 MeV. In 1983, a second microtron was added, upgrading the facility to

MAMI-A2 with maximum energy 183 MeV. With the addition of a third microtron in 1990, the maximum energy was increased to 855 MeVunder the name *MAMI-B. MAMI-C*, which is the present facility, was set into operation in December,2006 producing a continuous high quality electron beam with maximum energy 1.5 GeV. It supplies the electron beam to any of the experimental halls *(A1, A2, A4, X1*)as shown in Fig. 4.2.

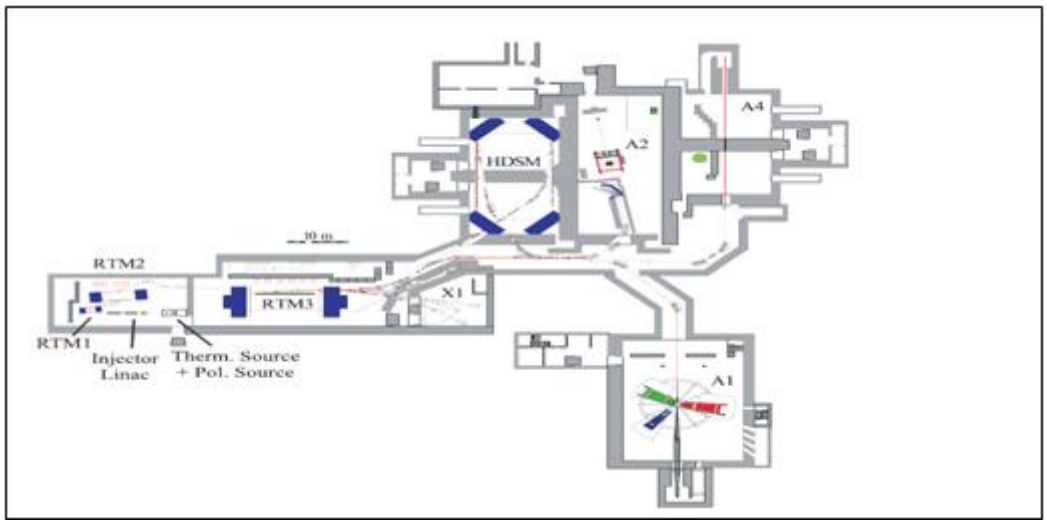

Figure 4.2: The floor plan of the accelerator and the experimental halls in the Institute fur Kernphysik, in Mainz [16].

MAMI-C consists of three cascades of *RTMs (Race Track Microtrons)* and a recently added *Harmonic Double-Sided Microtron (HDSM).* This new *HDSM* is considered as a worldwide unique recirculation electron accelerator. It consists of two systematic pairs of 90°-dipoles, each forming an achromatic 180° bending system as shown in Fig. 4.3. In order to compensate for the strong vertical defocusing due to the 45°-pole face inclination at beam entrance and exit, these dipoles incorporate an appropriate field gradient normal to the pole edge. This functions as a scheme for transversal focusing, with only two quadrupole doublets on each of the two dispersion-free anti-parallel linac axes. In the *HDSM*, the two linacs operate at different frequencies: one at 2.45 GHzand the other at 4.90 GHz. The linac operating at the lower frequency maintains a higher longitudinal stability. The linac at the higher frequency is responsible for a synchronous acceleration energy gain per turn below 20 MeV[22]. For the *HDSM*, the electron energy gained per turn is given by

$$\Delta E/\text{turn} = n \times [ecB/(\pi\text{-}2)] \times \lambda_{rf}$$

where n is the number of complete turns made by electrons (n = 1 is the lowest possible value) and λrf is the rf-wavelength. The injection of the electrons is made from the result of RTM3 (MAMI-B) with the value of B = 1.23 T, λrf= 0.1224 m; thus, from Eq. (4.1), ΔE = 41.1MeV/turn. This also needs 20 m long linacs, which would not fit into the existing MAMI-floor, as shown in Fig.4.2. Moreover, it would consume four times the electric power of MAMI-B. So it is practicable to adjust the frequency of the *HDSM* at 4.90GHz (λrf= 0.0612 m) with a small variation in B value as 1.823 T, to keep the length of the linacs about 10 m and the other parameters similar to that of *RTM3.* The *HDSM* takes the beam energy from 855MeV to 1508 MeV by 43 turns in 14.0 to 16.7 MeV per step through its accelerating section.

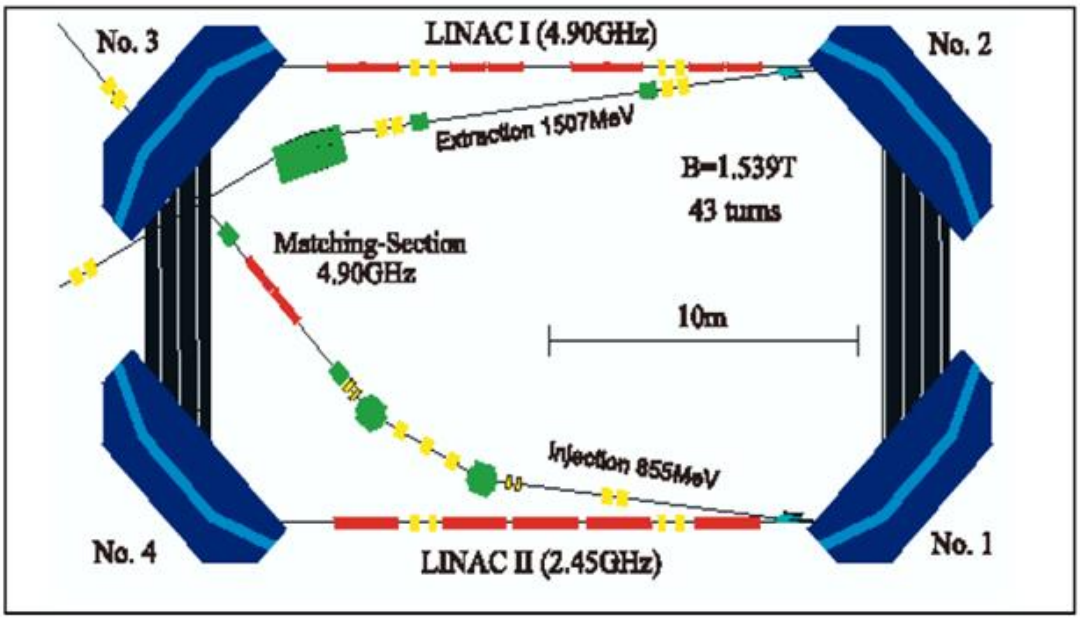

Figure 4.3: General layout of the HDSM. It consist mainly two pairs of 90° bending magnets and two linear accelerators. These two accelerators work on two different frequencies, 2.45 GHz and 4.90 GHz [17].

4.2 The Crystal Ball

The *Crystal Ball (CB)* was designed in 1974 as a multiphoton spectrometer with high detection efficiency over a large solid angle. It was initially used to detect photons produced in high energy e−e+ collisions [27] at *SLAC (Stanford Linear Accelerator Center in Stanford, CA).* From 1978 to 1981, it was used to investigate the spectroscopy of the J/Ψ and radioactive decays of particles such as τ ,Ψ, and D at SPEAR. After this period, it was put into storage at *SLAC* until 1995 when it was

moved to the AGS facility at *BNL*, where it was used for the study of nucleon and hyperons spectroscopy, and rare η decays. It was moved to Mainz in 2002 and after completion of a major upgrade of the detector's electronics it was used at *MAMI-B* until 2005. It resumed operation in 2007 as the central detector at *MAMI-C.* The *CB* consists of 672thallium-doped sodium iodide *NaI (Tl)* crystals. These crystals are optically isolated from one another by wrapping them in reflecting paper and aluminized mylar. A *SRC L50B01* type photomultiplier tube *(PMT)* of 5.1 cm diameter and 21 cm in length is arranged behind each crystal to convert the resulting light pulse into electric signals. Each crystal is shaped like a truncated pyramid of length 40.6 cm (or 15.7 radiation lengths) with the side of inner face 5.1cmin length and the side of outer face 12.7 cm as shown in Fig. 4.4. These crystals are arranged to form a ball structure as shown in Fig. 4.5 with an inner radius of 25.3 cm and outer radius of 66cm.

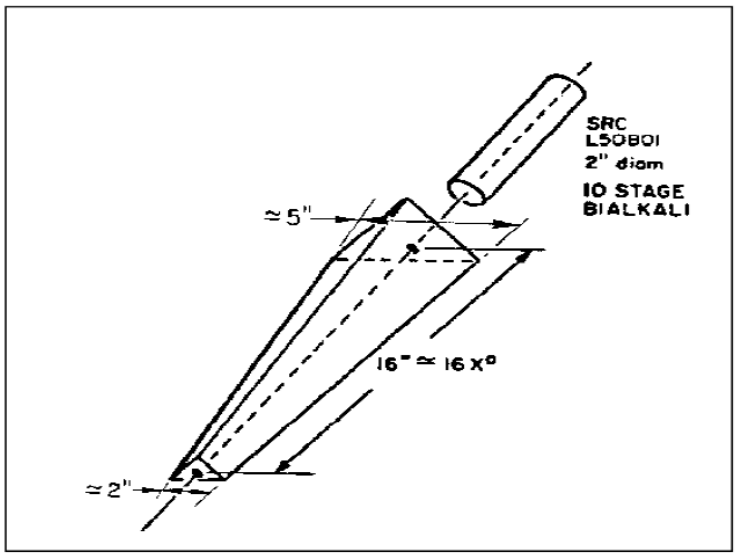

Figure 4.4: An individual crystal in the CB is 40.6 cm long with truncated pyramid shape [18].

The geometry of the *Crystal Ball* is that of an *icosahedron* (a solid with 20 faces). These **20** faces form "major triangles" which in turn are divided into faces of four "minor triangles" each containing nine crystals as shown in Fig. 4.6. When these crystals are stacked together closely they form a spherical shell of 720 elements. In order to make a space for the photon beam and the target system, 24 crystals were removed from the opposite poles. The *CB* is divided into two hemispheres: an upper one and a lower one separated with two 0.8 mm stainless steel plates and a 0.8 cm air

gap. Because of this, an active space amounting to 1.6% of the solid angle (or 4π) is introduced. Since *NaI (Tl)* is hygroscopic, all the crystals are hermetically sealed in the two separated hemispheres. This also helps to control the temperature (23 ± 2° C), pressure (low) and humidity (∼30%) inside the hemispheres. In the *Crystal Ball*, the

incident photon beam produces electromagnetic showers that in turn deposit their energy in the *NaI (Tl)* crystals depending on the energy of the photon. An incident photon below 10 MeVmay deposit energy only in one or two crystals whereas a photon up to 400 MeVdeposits 98%of its energy in a cluster of 13crystals. Because of this, the measurement of photon energy from the *Crystal Ball* is considered quite precise and the energy resolution is taken as

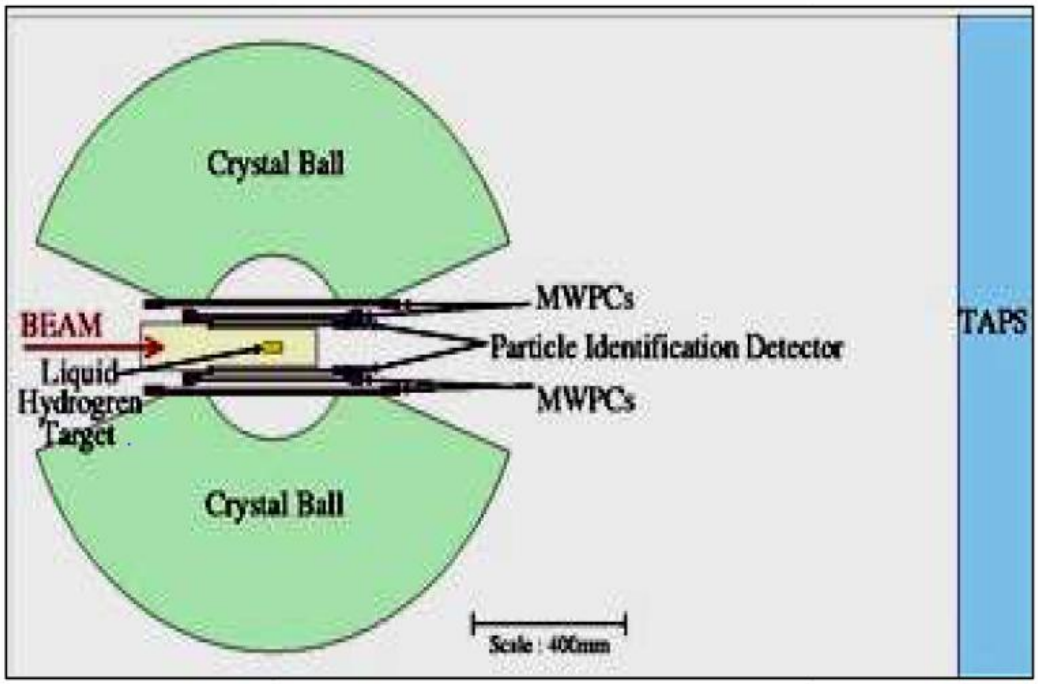

Figure 4.5: A transverse view of the Crystal Ball showing the sub detectors inside it. A liquid hydrogen target is also located at its center [17].

Because of the high granularity of the resolution. For hadrons and charged particles, the positional resolution is not optimal as the hadronic shower has less transverse extension. Thus for charged particles other additional detectors are required. Some of the important properties of the Crystal Ball are listed in Table 4.1.

Table 4.1 Geometrical properties of the Crystal Ball [16].

Azimuthal angular acceptance	$0° \leq \phi \leq 360°$
Polar angular acceptance	$20° \leq q \leq 160°$
Azimuthal Angular resonance (σ_θ)	$(2\text{-}3°) / \sin q$
Polar angular resolution (σ_φ)	$2\text{-}3°$
Photon Energy Resolution (σ_E/E)	2.05% $E\ (GeV)0.36$

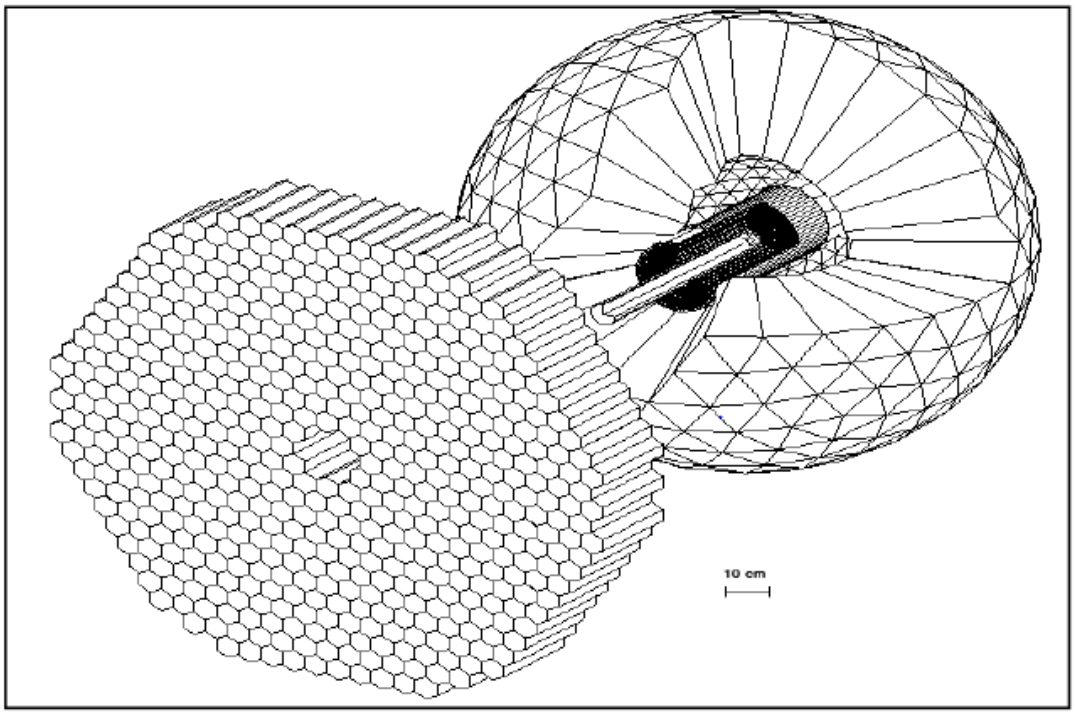

Figure 4.6: The use of TAPS as a forward wall detector at a distance 1.8 m from the CB. The 384 BaF_2 crystals of the TAPS forward wall cover the hole of the CB to cover ~96% of 4π in solid angle [16].

Because the relative intensity of the short component is higher for photons than for nucleons, the ratio of these two components provides a good tool to identify these particles as shown in Fig. 4.6. Third, *BaF2* has a high photon detecting efficiency and energy resolution over a wide range of energies. In addition, because of the high granularity of *TAPS*, there is a good position resolution.

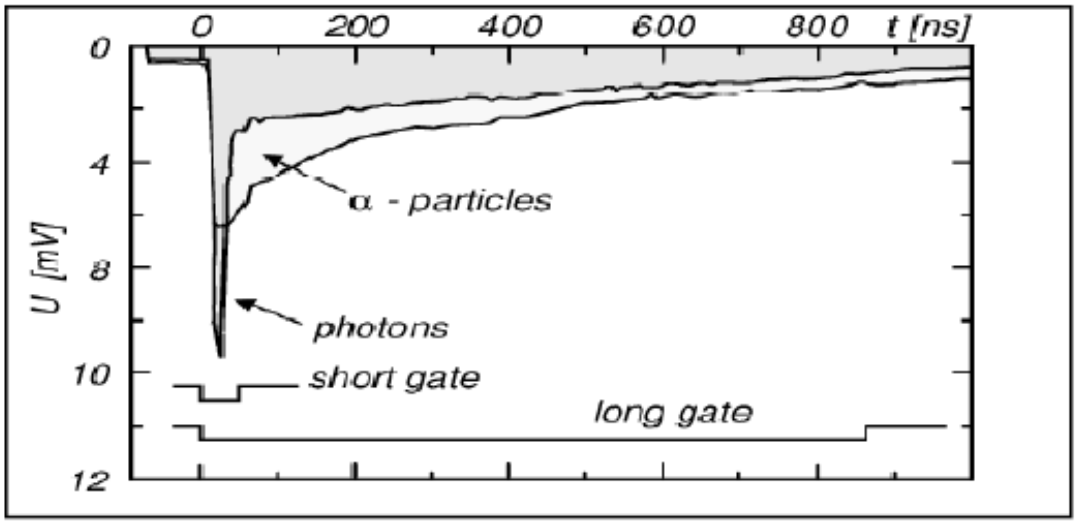

Figure 4.7: A schematic plot of the pulse shape for an α -particle and a photon in TAPS. The larger long component makes it possible to distinguish the α –particle and a photon [18].

Each of the *BaF2 detectors* has hexagonal front and back shapes with a cylindrical end part of inner diameter 5.9 cm as shown in Fig. 4.8. The surfaces of the crystals are polished. A UV reflector that is made up of eight layers of *PTFE3* and one layer of thin aluminum foil is wrapped around these crystals. The individual crystals are coupled to a Hamamatsu *R2059* photomultiplier tube using silicon egrease. In order to provide effective magnetic shielding up to a flux of 0.02T, the phototubes and the cylindrical section of the crystals are completely surrounded by a magnetic shield. In front of each *BaF2detector*, a hexagonally shaped *5 mm* thick NE102A plastic scintillator is installed so as to distinguish between charged and neutral particles. These are called veto detectors. Some of the important properties of the TAPS detector are summarized in Table 4.2.

Table 4.2: Properties of TAPS [16]

Distance from the center of CB	*1.80 m*
Polar angular acceptance	$2^0 \leq \theta \leq 20^0$
Time resolution	*0.5 ns FWHM*
Angular resolution (σφ)	0.7^0 *FWHM*
Energy Resolution (σE / E)	$3.7\%/E\ (GeV)^{1/4}$

CHAPTER 5

Data Analysis

This chapter explains the *analysis* software and Monte Carlo simulation used for our present work. For our dissertation, first we setup root environment in Linux 14.04.All files were run in terminal. For photoproduction reaction $\gamma p \rightarrow \eta p \rightarrow \gamma\gamma p$ we choose suitable *.dat*file, and made several *.dat*files for different energy of striking gamma. Now these files were moved into *.hbook*. Again, these files made under *.hbook* were run to give *mkin* files. These *mkin* files were run under *cbsim* . These *cbsim* files were again run in *acqu*. From the histograms obtained from *acqu,* we studied photoproduction reaction $\gamma p \rightarrow \eta p \rightarrow \gamma\gamma p$.

5.1 Analysis software

5.1.1 ROOT

The root system provides a set of frameworks with all the functionality needed to handle and analyze large amounts of data in a very efficient way. Having the data defined as a set of objects, specialized storage methods are used to get direct access to the separate attributes of the selected objects. This allows the easy setup of an analysis system without having in touch the bulk of the data that can query and process the data interactively. *ROOT* also provides a good environment to learn *C++*. *ROOT* helps to built acquisition, simulation and data analysis systems [26].

5.1.2 Importance of ROOT

The *ROOT* project was started as an analysis tools for the experiment of *CERN*. With *ROOT,* we can try to provide a basic framework that offers a common set of features and tools for all domains of high energy physics computing. Currently the emphasis of *ROOT* is on the data analysis. The system can easily be extended to other domains like simulation, reconstruction and event displays. *ROOT* is an ideal environment to introduce physicists quickly to the new world of objects and C++ [27].

5.2 *AcquRoot*

AcquRoot is the analysis software that is used for all of the online and offline analysis of data for *Crystal Ball* experiments at *MAMI*. It is an upgraded form of *ACQU*

incorporating with the multi-threaded purely *C++* program mainly written by J. R. M. Ann and [29]. *AcquMC* is a Monte Carlo reaction kinematics generator and *AcquDAQ* reads data from some components of the detector system and feeds the data to one or more central event builders. AcquRoot is based on the framework of *ROOT* [27], which is the *CERN C++* based suite of software and libraries. *ROOT* is based on object-oriented sources, comprised of various types of classes, each performing a specific task. As *AcquRoot* combines the full *ROOT* functionality, it makes extensive use of the facilities offered by *ROOT* for controlling *A2 electronics*, data acquisition, storage, retrieval, and analysis. The tree structure of the *AcquRoot* analyzer is shown in Fig. 5.1.

The four circles of different colors on the left-hand side of the figure represent the four important classes involved in *AcquRoot*. The lowest green circle represents a dedicated class specific to each detector: e.g., *Crystal Ball NaI* crystals detectors are accounted by the class *TA2CBNaI, TAPS BaF2 crystals* by *TA2TAPS BaF2*, focal plane tagger detectors by *TA2TaggLadder* and so on. These detector classes are responsible for conversion of the digitally stored pulse heights to energies and times. The blue circle, one step higher, represents the three classes that collect information from each of the three subgroups of the detectors. *TA2CrystalBall* represents the group of detectors related to the *Crystal Ball*. Similarly, *TA2TAPS* and *TA2Tagger* represent all the detectors related to the *TAPS* (e.g., *BaF2, Veto*), and *the Tagger* (e.g., *Ladder, Pb Glass, Micro*), respectively.

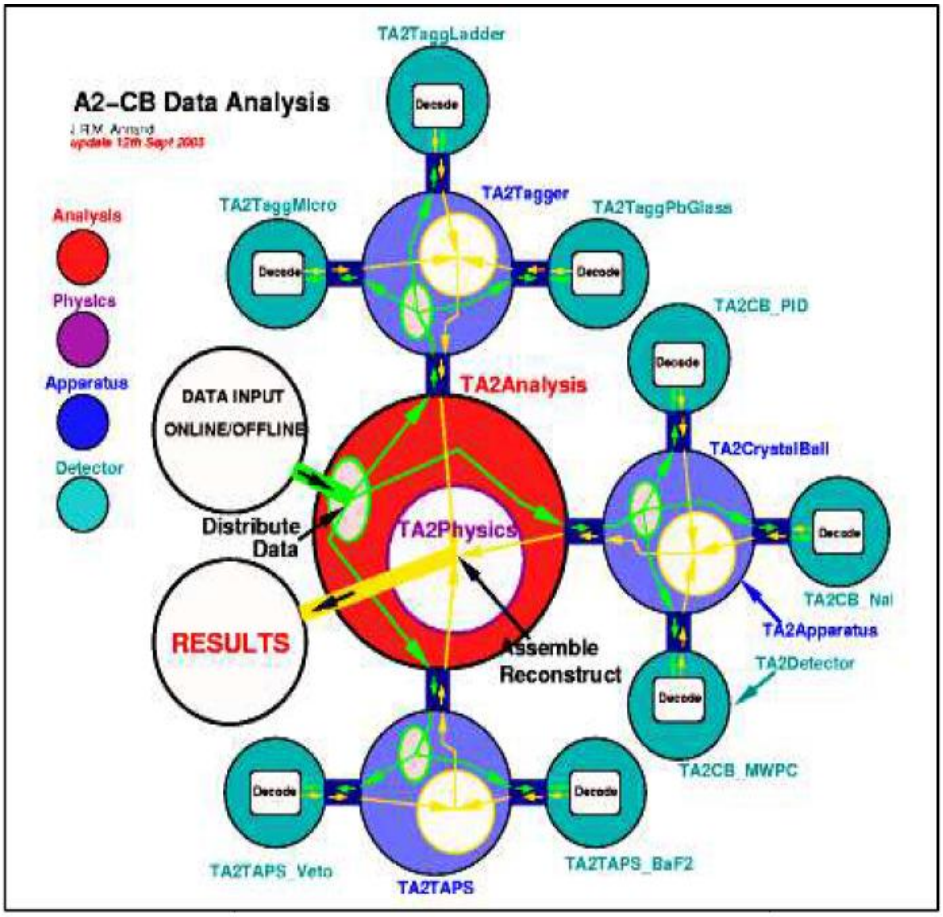

Figure 5.1: The tree structure of *AcquRoot* Analyser with its Apparatus ,Detector, Physics and Analysis classes [29].

These three classes in a group form a class called*TA2Analysis*which is responsible for the conversion of energies and times into particle types and four vectors. The pink circle above the blue circle represents a Physics class that collects all the information from the three detector systems (such as four vector and particle-identities) to reconstruct the related events yielding the invariant and missing mass to identify the specific particle. The red circle on the top represents a class called*TA2Analysis*which provides the core of the data analysis system. It decodes the basic *ADC, TDC*, and *Scalars information* and passes them to *TA2Apparatus*

5.3 Monte Carlo simulation

Monte Carlo methods (or **Monte Carlo experiments)** are a class of computational algorithms that rely on repeated random sampling to compute their results. Monte Carlo methods are often used in computer simulations of physical and mathematical systems. These methods are most suited to calculate computer and tend to be used

when it is infeasible to compute an exact result with a deterministic algorithm. This method is also used to determine theoretical derivations.

Monte Carlo methods are especially useful for simulating systems with many coupled degrees of freedom, such as fluids, disordered materials, strongly coupled solids, and cellular structures. They are used to model phenomena with significant uncertainty in inputs, such as the calculation of risk in business. They are widely used in mathematics, for example to evaluate multidimensional definite integrals with complicated boundary conditions. When **Monte Carlo simulations** have been applied in space exploration and oil exploration, their predictions of failures, cost overruns and schedule overruns are routinely better than human intuition or alternative "soft "methods.

There were two parts to the **Monte Carlo simulations**, the *event generation* and the *particle tracking.*

As the first step, a program was used to generate the kinematics of events. The input parameters were the target dimensions, mass, and density, also the beam energy, spot size at the target, as well as the beam divergence, for this we used real "beam triggers "recorded in the course of the experiment.

The second step used a program based on the *CERN package GEANT, version3.21*, that reads the output of the first program and tracks all particles through volumes of different materials, in a setup that mimics as closely as possible the actual experimental setup. The geometries included were the *CB; TAPS, TAPS veto wall, PID* and *the target* (see chapter 4) [29].

This chapter presents the study of photoreaction $\gamma p \rightarrow \eta p \rightarrow \gamma\gamma p$. In this events for $\gamma p \rightarrow \eta p$ were simulated using the **Monte Carlo analysis**. Since the threshold, photon energy for $\gamma p \rightarrow \eta p$ is 702.77 MeV **(**see chapter 3.4), we have to provide energy of incident photon beam just greater than threshold energy for η meson production [26]. The ηp final state is obtained through the following sequential decays:

$$\gamma p \rightarrow \eta p \qquad (5.1)$$

and η further decays into two γ as

$$\eta \rightarrow \gamma\gamma \qquad (5.2)$$

so our final decay becomes

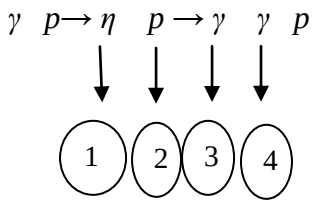

(5.3)

Where,

1 ⇒eta produced as first particle

2 ⇒Proton produced as second particle

3 ⇒Gamma produced as third particle

4 ⇒Gamma produced as fourth particle

With reference to the threshold energy, we create an environment to provide energy of photon more than threshold i.e. more than 702.77 MeV. In our study we started from 710 MeVand within the interval of 40i.e. 750, 790, 830, 870, 910, 940,980, 1020, 1070, 1110, 1150,1190, 1230, 1270, 1310, 1350, 1390, 1430,1470and 1510MeVdata were taken.

In our reaction $\gamma p \rightarrow \eta p \rightarrow \gamma\gamma p$ particle are kept according to

GEANT *id* such that

$$\gamma = 1$$

$$p = 14$$

$$\eta = 17$$

For the reaction $\gamma p \rightarrow \eta p \rightarrow \gamma\gamma p$ we have to provide suitable value of photon energy ≥702.77MeV. That beam of photon is incident on *liquid hydrogen target* and produces two *photons* and *proton*. Since we are doing this process through simulation, we provide such environment through *dat*file. One of the examples of *dat*file is shown in Appendix [A.1].

We made several *dat*files. Now these made files were run under *./deck_kin*in*mami_mcarlo/deckin*. The high-energy photon incident on *liquid*

hydrogen target 50000 times. The events were generated for each energy value from 710 MeV to 1510MeV**.** After that, we move these files to *results_deckin*. Where we used command e.g

mv ._hbook ../results_deckin/deckin_newetagama_710.hbook

*mv _.hbook ../results_deckin/deckin_newdevshree_710.hbook*etc

These files made under *hbook* are converted into root files using command

```
h2rootnew_devshree.710.hbooknew_devshree.710.root
```

or simply other files converted by using following command [29].

```
h2root new_devshree.%.hbook new_devshree.%.root
```

Where % represents any value of the energy range 710 to 1510 MeV that were included in the dat files. '*new_devshree.710.root*' is the one example of root files at energy 710MeV. This root files is being opened in the root program by using the following code;

*'root new_*

```
rootnew_devshree.710.root'

'newTBrowser'
```

While this file in the '*root*' is opened by using the code '*new TBrowser*'; we obtained the different histograms for the energy 710MeV [23].

5.4 Event generation by using *mkin* software

After converting *hbook* files into *root* files we study whether the basic needs for our reaction is fulfilled or not. By studying the nature of histograms obtained from *root* files, we can conclude that events are generated according to our photoreaction $\gamma p \rightarrow \eta p \rightarrow \gamma\gamma p$. Actually all *root* files corresponding to different *dat*files for each energy values generate events. Among them, one *root* file corresponding to energy value *1510 MeV* is taken as example. In this *root* file, we can see different histograms, which are depicted below.

5.4.1 Generation of ηmeson as particle (1)

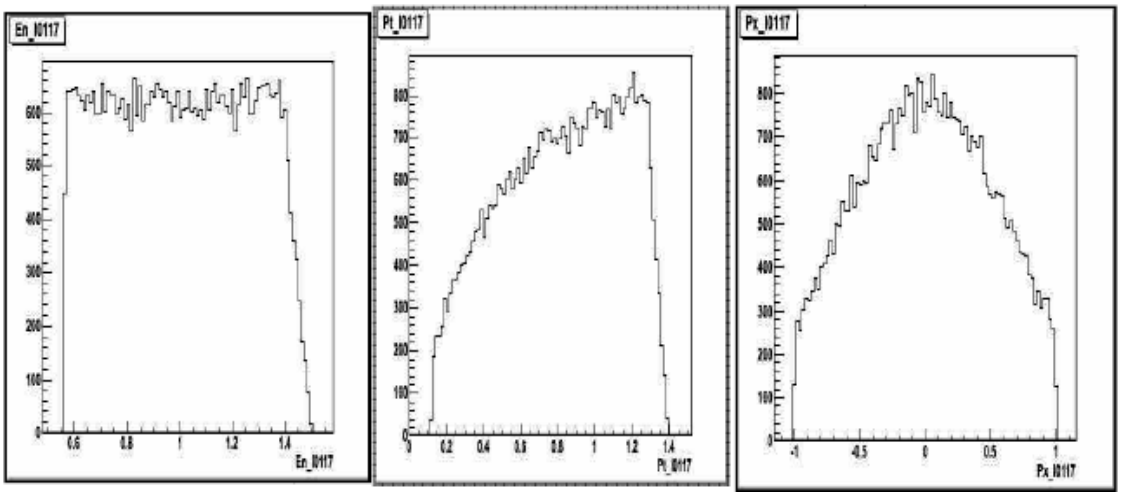

Figure 5.4: Energy of eta meson produced as particle (1) **Figure 5.5:** Transfer momentum of eta produced as particle (1) **Figure 5.6:** Momentum of eta along x-direction as particle (1)

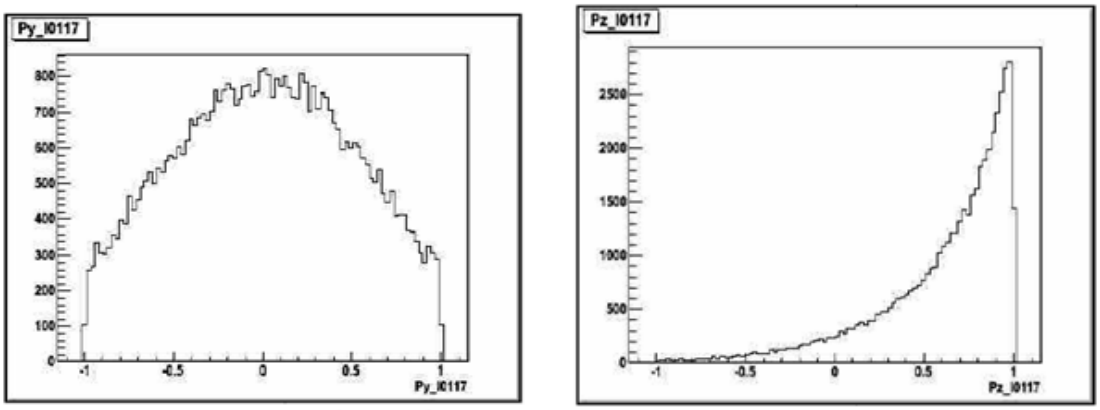

Figure 5.7: Momentum of eta along y-direction as particle (1) **Figure 5.8:** Momentum of eta along z-direction as particle (1)

*Reffering to Eq.(5.3)*we have provided environment to the photoreaction $\gamma p \rightarrow \eta p \rightarrow \gamma\gamma p$ in *.dat*file. According to this reaction,η was first produced particle.Figures 5.4 to 5.8 show that eta meson produced as first particle. In each figures we can see a code as 10117**.** In these five figures code 17(last two digit in code) represent *eta meson* produced. Middle 1 in code 10117denotes first produced particle. En represents energy, P_t represents transfer momentum, P_x, P_y, P_z represents momentum along x-,y-,z-direction respectively in our photoreaction $\gamma p \rightarrow \eta p \rightarrow \gamma\gamma p$ *[8,27]*.

5.4.2 Generation of proton as particle (2)

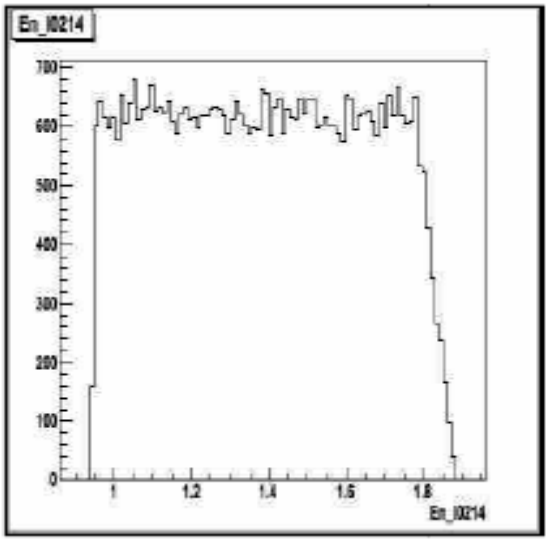

Figure 5.9: Energy of proton as particle (2)

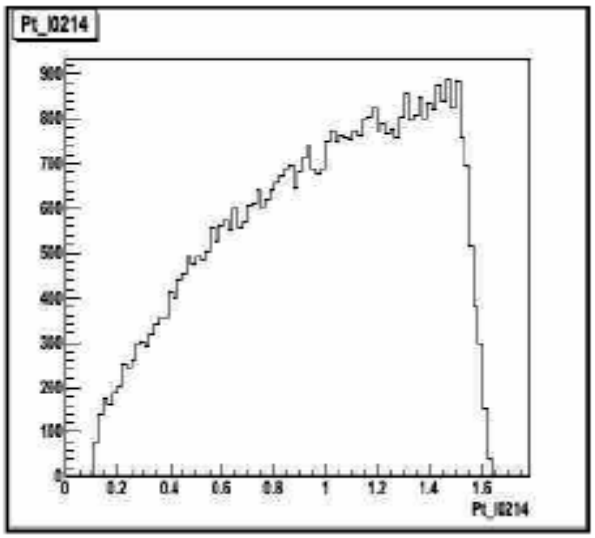

Figure 5.10: Transfer momentum of proton as particle (2)

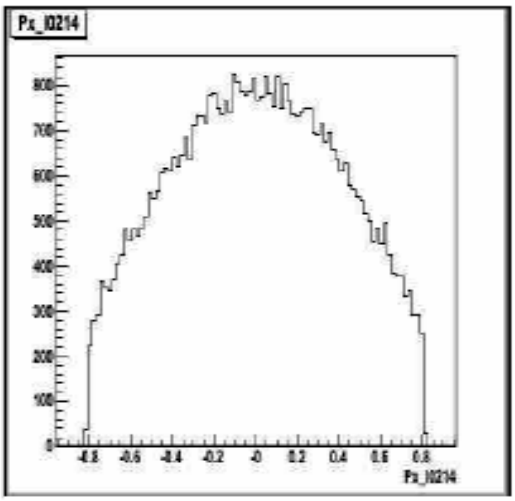

Figure 5.11 Momentum of proton along x-direction as particle (2)

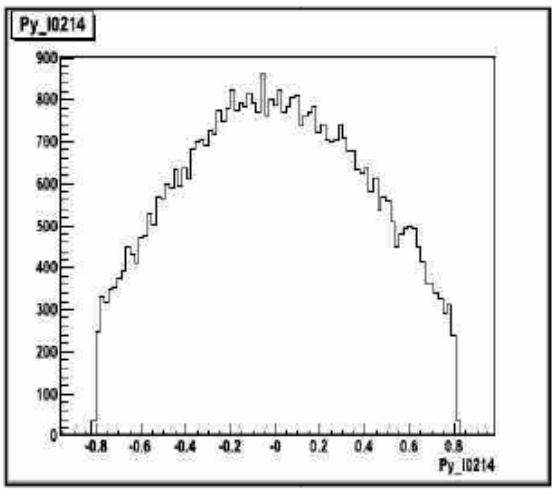

Figure 5.12: Momentum of proton along y-direction as particle (2)

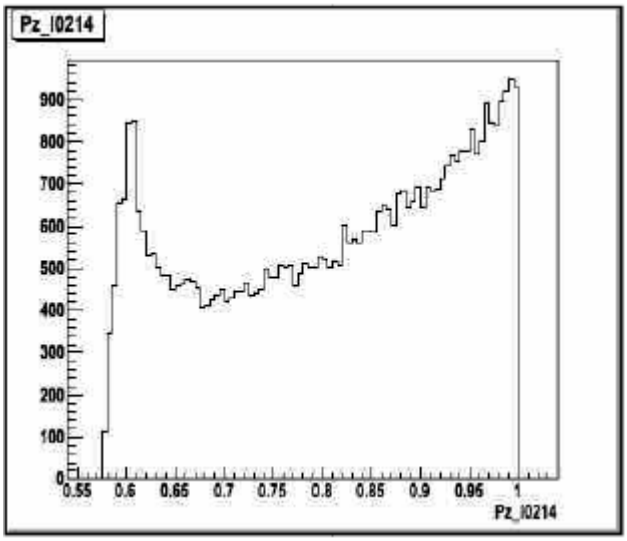

Figure 5.13: Momentum of proton along z-direction

as particle (2)

Considering the Eq. (5.3), proton was the second produced particle in the reaction $\gamma p \rightarrow \eta p \rightarrow \gamma\gamma p$. In the histograms obtained from *root* file proton can be seen as second produced particle. In above figures code-10214, 14 refer to GEANT id of proton and middle 2 in 10214 represents second produced particle. En represents energy, Pt represents transfer momentum, Px, Py and Pz represents momentum along x-, y- and z-direction respectively in our photoreaction $\gamma p \rightarrow \eta p \rightarrow \gamma\gamma p$

5.4.3 Generation of gamma as particle (3)

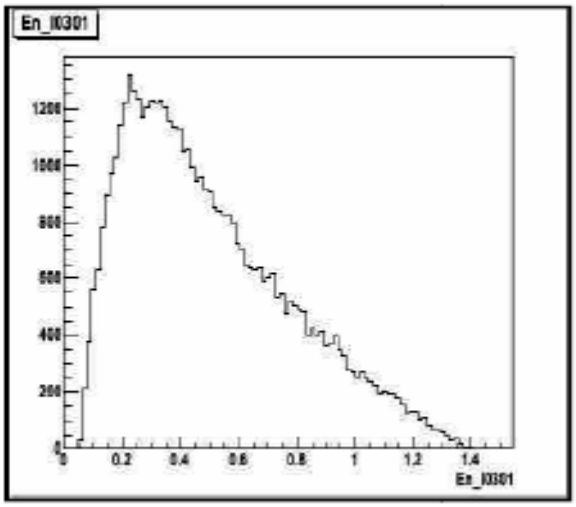

Figure 5.14: Energy of photon produced as particle (3)

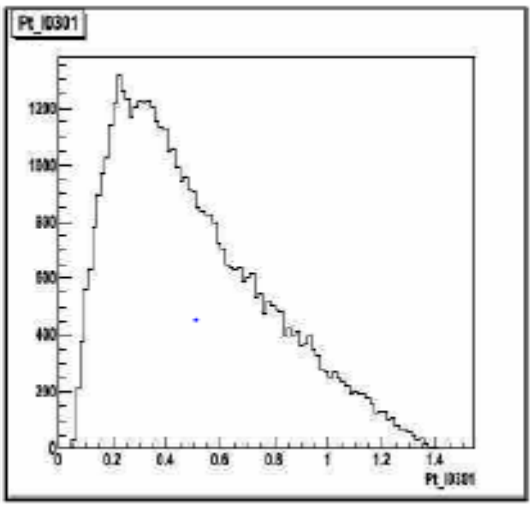

Figure 5.15: Tranfer momentum of photon produced as particle (3)

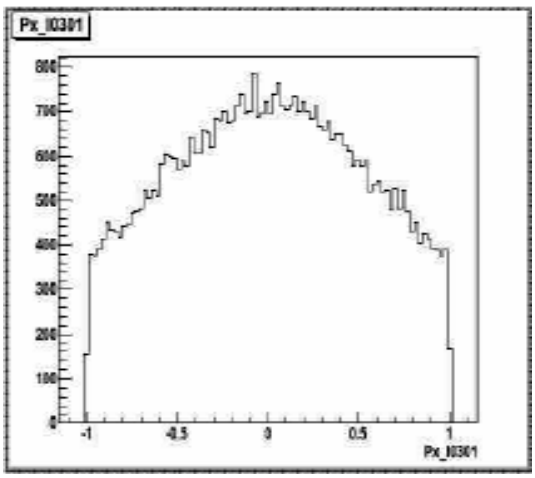

Figure 5.16: Momentum of particle along x-direction as particle (3)

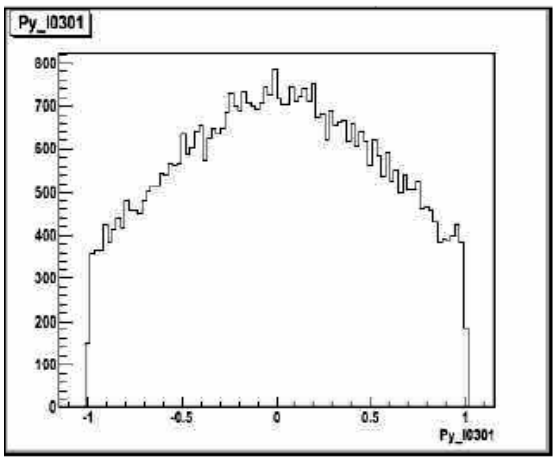

Figure 5.17: Momentum of particle along y-direction as particle (3)

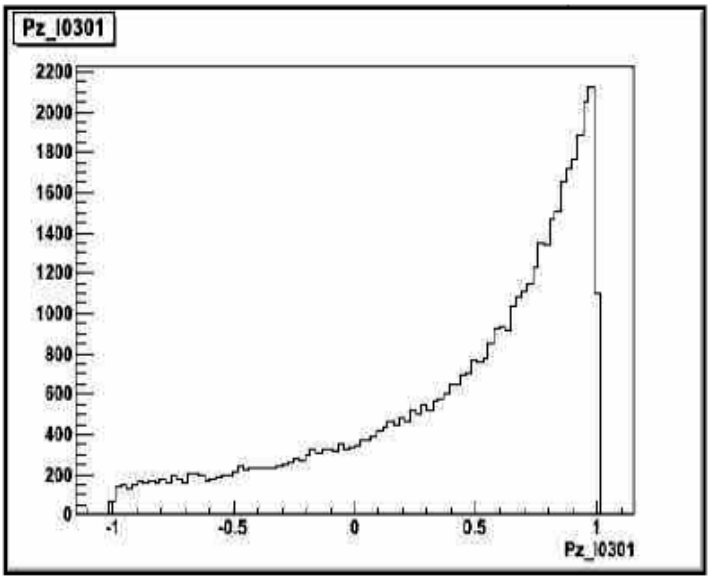

Figure 5.18: Momentum of particle along z-direction as particle (3)

Referring to Eq.(5.3),we have provided an environment to the photoreaction $\gamma p \rightarrow \eta p \rightarrow \gamma\gamma p$ in *.datfile.* According to this reaction, photon is the third produced particle Figures 5.14 to 5.16 photon was produced as third. The GEANT id of photon is 1.In these five figures code 10301(the last two digit 01in code) represent photon was produced. Digit 3 in each code 10301 denotes third produced particle. E_n represent energy, P_t represent transfer momentum, P_x ,P_y and P_z represents momentum along x- ,y- and z-direction respectively in our photoreaction $\gamma p \rightarrow \eta p \rightarrow \gamma\gamma p$. The nature of energy histogram and transfer momentum histogram are exactly similar. This indicates that energy is transferred into momentum.

5.4.4Generation of gamma as particle (4)

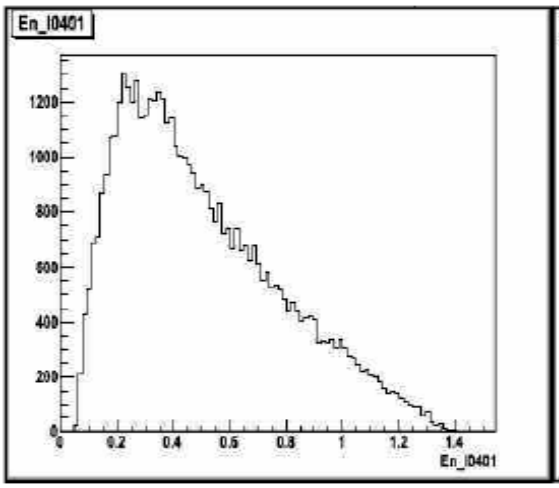

Figure 5.19: Energy of photon produced as particle (4)

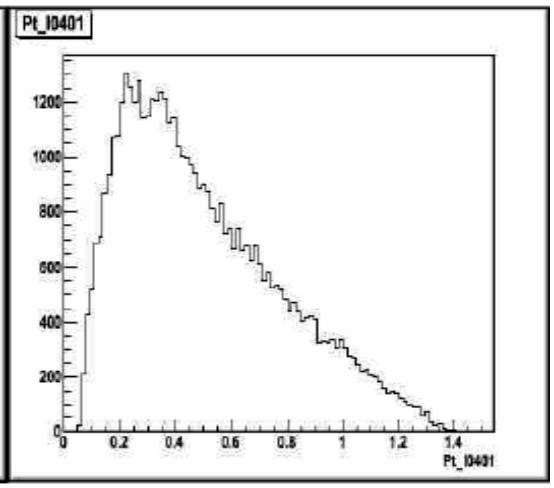

Figure 5.20: Transfer momentum of photon produced as particle (4)

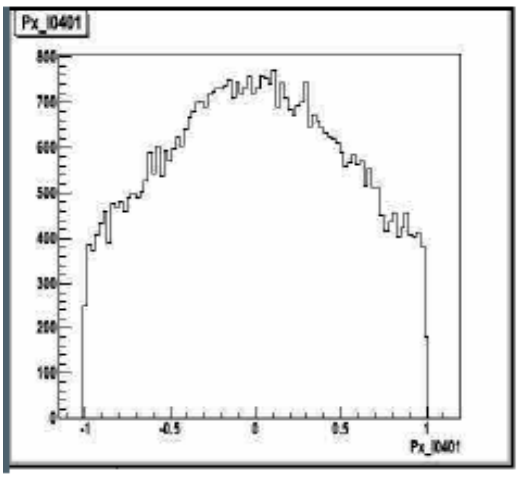

Figure 5.21: Momentum photon along x-Direction as particle (4)

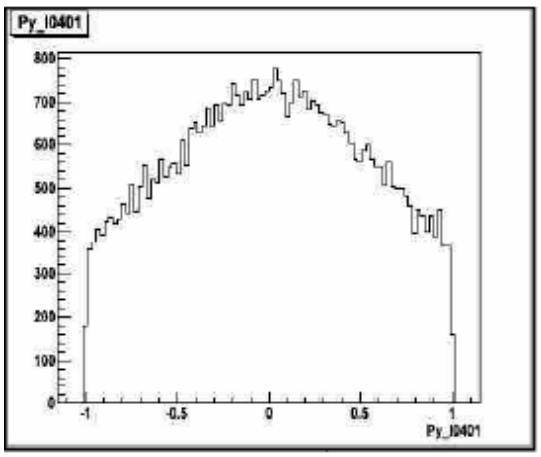

Figure 5.22: Momentum photon along y-direction as particle (4)

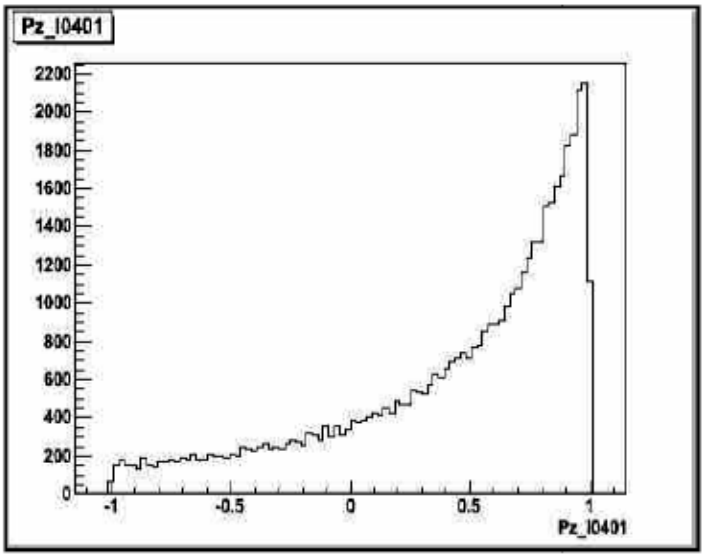

Figure 5.23: Momentum photon along z-direction as particle (4)

Above figures from 5.19 to 5.23 shows that photon was produced as fourth particle. In each figures the code 10401 is present. The last two digits 01 in 10401 represent GEANT id of photon and 4in 10401 represents photon was produced as fourth particle. En represents energy, P_t represents transfer momentum, P_x, P_y and P_z represents momentum along x, y and z direction respectively.

From the figures from 5.4 to 5.23 show that 4 particles were generated namely eta meson as (1) proton as (2), photon as (3) and another photon as (4).

In these figures the nature of energy histogram and transfer momentum histogram are similar which indicates that the energy is transferred to the momentum.

5.4.5 Generation of photon beam

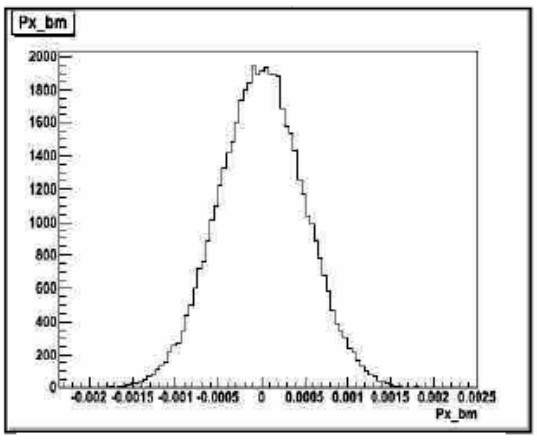

Figure 5.24:Momentum of beam along x-direction

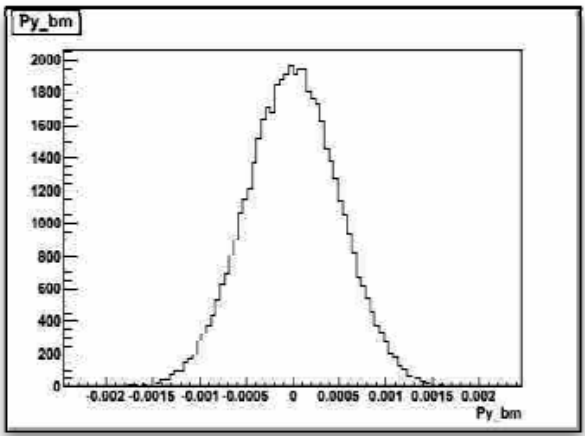

Figure 5.25: Momentum of beam along y-direction

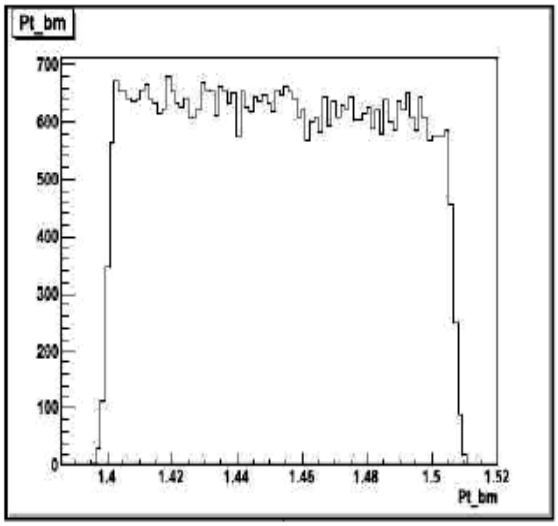

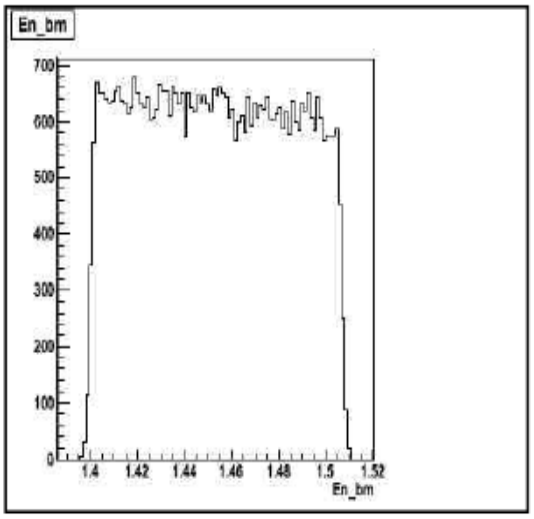

Figure 5.26: Transfer momentum of beam

Figure 5.27 Energy variation of beam

Above figure from 5.24 to 5.27, show the nature of incident beam of photon. Fig.5.24 and Fig. 5.25 show the momentum of beam along x- and y- direction respectively. Fig 5.26 and Fig. 5.27 show the transfer momentum of beam and energy of beam. The nature of energy variation of beam and transfer momentum of beam is quite similar. This indicates that the energy of beam is transferred to the momentum in the photoreaction Eq. (5.3).

5.4.6 Generation of target vertex

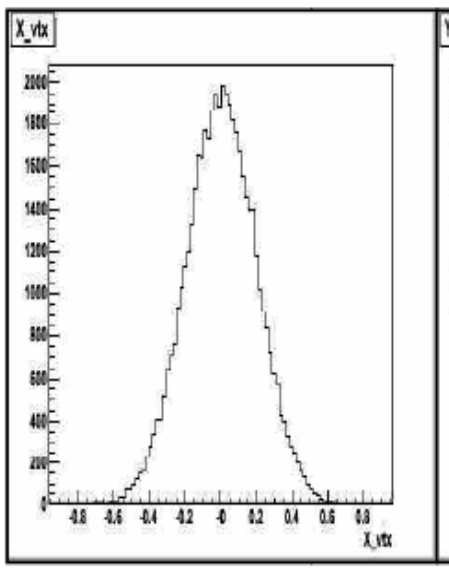

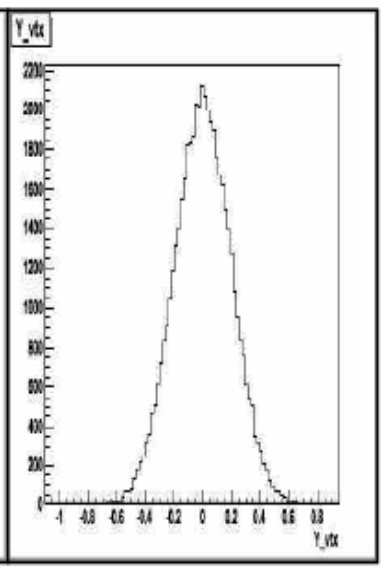

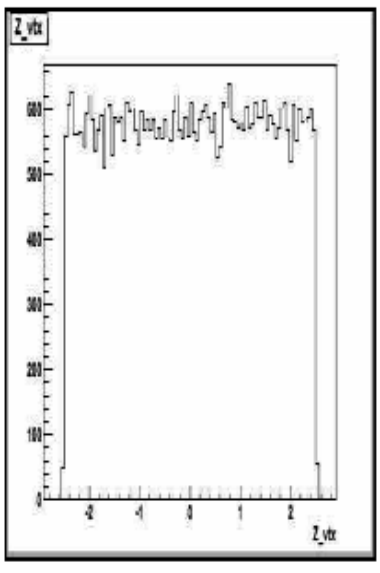

Figure 5.28: X- vertex

Figure 5.29: Y- vertex

Figure 5.30: Z-vertex

Above figures from 5.28 to 5.30 show the vertices made along x- direction, y-direction and z- direction when beam of photon incident on the target in the photo reaction γp → ηp → γγp. The nature of vertex made along x- and y- direction is found similar.

5.5 Event identification by using *cbsim* software

The files generated in *deckin* files are detected by using *cbsim* software. For this, we have to run these *mkin* files into *cbsim.* In *mkin* file, we made necessary correction. We choose *gamaeta.ffcards*files in *mkin.* One mkin file is as shown in Appendix [B.1].

In *mami_mcarlo/jb_ffcards files/gamaeta_ffcards*files Appendix [C.1] we choose suitable *TRUE/FALSE* option according to our reaction.

Then we run our files using command *./mkin_run_good.sasha.e.g* which represents energy values 710MeV, 750MeV, or 790MeV...1510MeV**.** After running these files, we check the particles through their **GEANT** id (See Table 1.3). Results of *cbsim* file in form of histograms are shown in Fig. 5.31 to Fig.5.40 below.

5.5.1 Particle identification

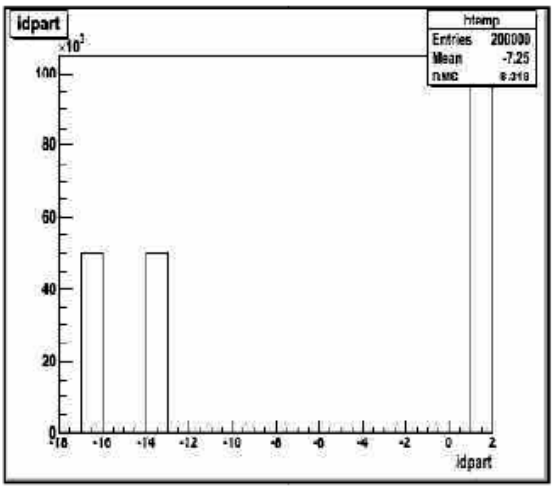

Figure 5.31: Identification of produced particle in γp → ηp →γγp

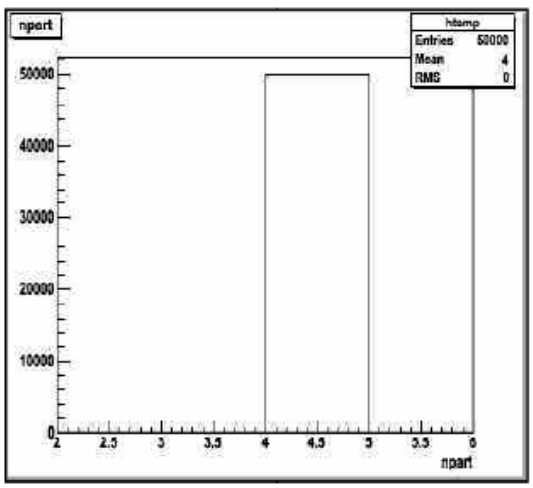

Figure 5.32: Number of particles produced in γp → ηp →γγp

Fig.5.31 shows that the identification of particles in the reaction γp → ηp →γγp. Histogram 5.32 shows there is height at points 1, 14 and 16. 1 means **GEANT** id of

photon, 14 means **GEANT** id of *proton* and 17 means **GEANT** id of *eta meson*. This means we had used these three particles in *.dat*file. These particles are detected in *cbsim*. Fig. 5.32 shows that number of particles involved in *eta* meson photoproduction. There is starting of height from point 4, it means 4 particles were involved in the reaction $\gamma p \rightarrow \eta p \rightarrow \gamma\gamma p$. These two facts detected as true because the same number of particles i.e. 4 and same particles i.e. *eta meson, proton* and *photon* are producing that also were used in *.dat*file.

5.5.2 Vertex identification

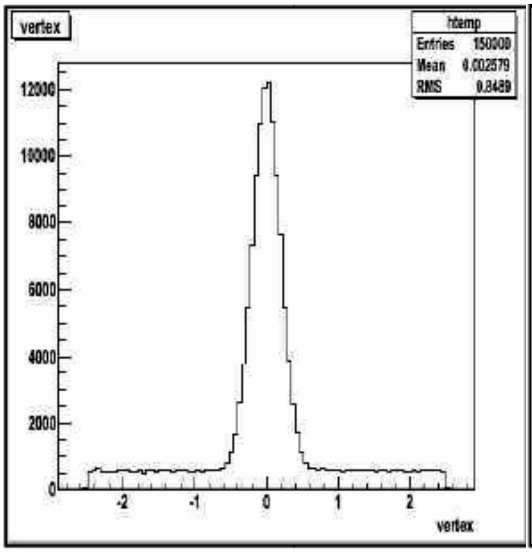

Figure 5.33: Vertex made by hitting the target by incident photon

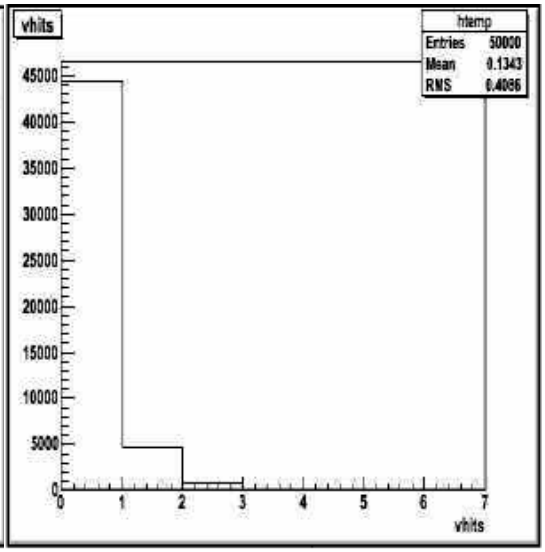

Figure 5.34: Maximum hit by gamma to the target

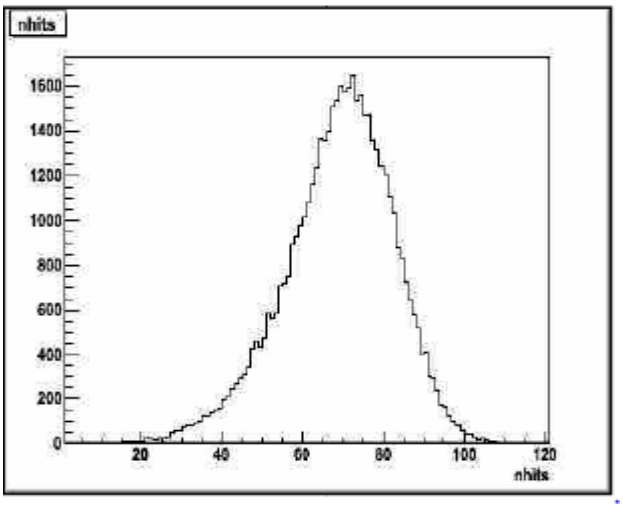

Figure 5.35: Number of times hit by beam of photon to the target in the photoreaction $\gamma p \rightarrow \eta p \rightarrow \gamma\gamma p$

Fig 5.33 shows the vertex made by hitting the target by photon beam. The peak is at origin implies that the incident beam mostly incident at the centre of the target. Fig. 5.34 shows that maximum hit by photon beam to the target. The height is maximum at origin implies that photon beam is incident at the centre of the target. Fig. 5.35 shows the average number of hits by the incident beam to the target. It shows the average number of hit is approximately 60.

5.5.3 Detection of energy and momentum

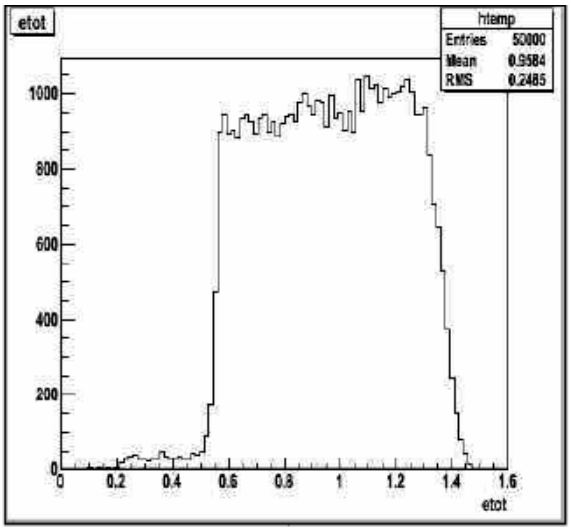

Figure 5.36: Total energy variation

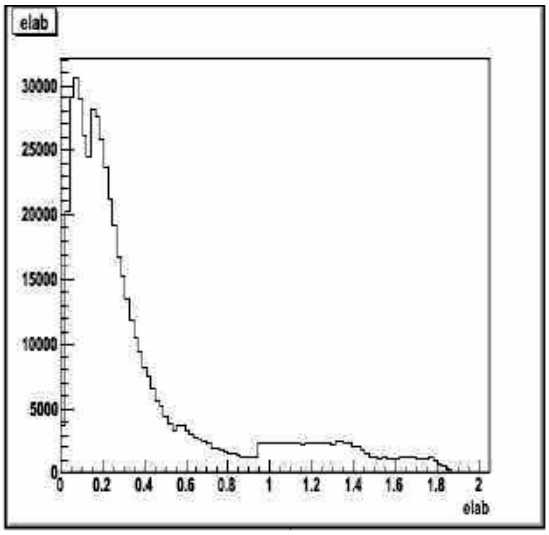

Figure 5.37: Distribution of energy variation in lab

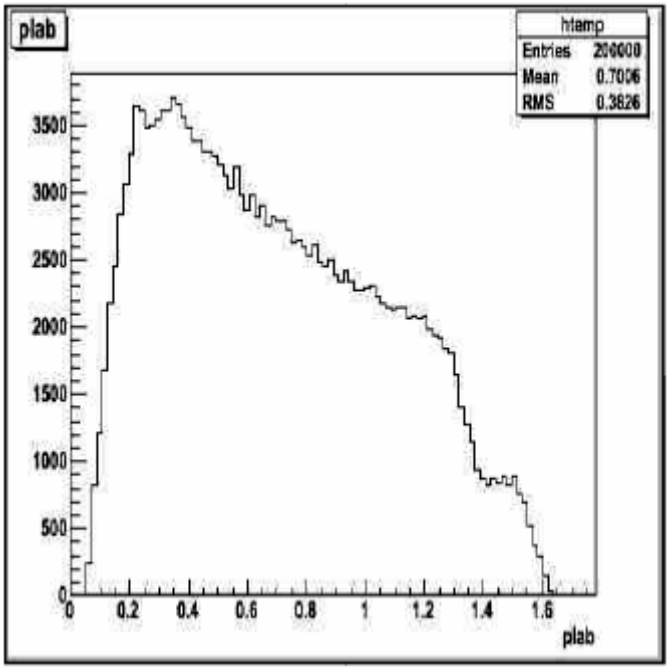

Figure 5.38: Distribution of momentum in lab

Fig. 5.36 shows the variation of total energy . This figure is similar to the Fig. 5.27 (energy of the beam). The same type of beam what is generated at *mkin* is detected at *cbsim* Fig. 5.37 shows that distribution of energy in lab and Fig. 5.38 shows distribution of momentum in lab.

5.5.4 Crystal Ball and TAPS detector as prime

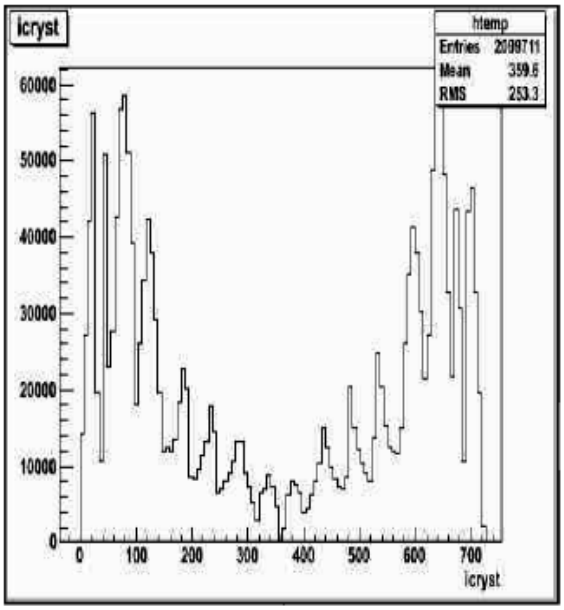

Figure 5.39: Position of elements of NaI crystal in Crystal Ball

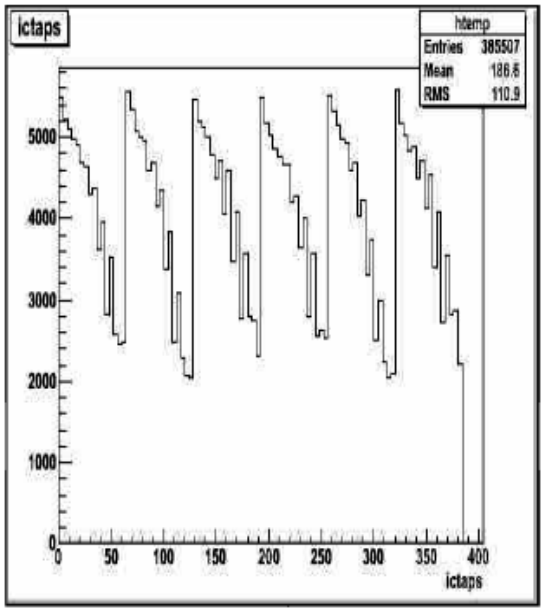

Figure 5.40: Position of elements of BaF_2 crystal in TAPS

Fig. 5.39 shows that the position of 720 elements of NaI crystal in *Crystal Ball.* Fig. 5.40 distribution of position of 384 elements of BaF2 crystal in TAPS.

From these figures from 5.29 to 5.38 we see that the files generated in *deckin* are detected in *cbsim*.

In above figures:-

Etot ⇒ total energy, id part ⇒ GEANT ids of particles involved in reaction

dircos ⇒ direction cosine

From id part figure we can see proton, eta and gamma are involved in our reaction.

Now we have to run these files in acqu. Before this, we have to make necessary correction in *acqu/root/src/TA2PhotoPhysics.cc*and*acqu/root/src/TA2 PhotoPhysics .h.*

Similarly energy range, mass range etc. correction were made in *acqu/data/CBphysics.dat.* Similarly, we provide the correct path and name in *acqu/data/CBMC.Offline.* One *CBMC* file is shown [D.1]and then we run our files in *acqu* using command *Acquroot --offline CBMC.Offline.* These files made in *acqu* are moved in *root* according to our name for easy detection of our files with their respective energy.

Now we see our result in *root*. In *root* we choose command *root* (our files name made in acqu) for different energy value of gamma. We check our result for one energy value. Similar steps were performed for all values of energy.

Next we have to merge these all files to get combined result in the energy range (710 MeV to 1510 MeV) .We change in *acqu/data/rootmerge.C*. First we make four combined result from 735 to 870, 910 to 1070, 1010 to 1270 and 1310 to 1510 MeV and then we finally combined these four files into one to get the combined result from the energy range 710 to 1510 MeV.

5.6 Reconstruction of events using *acquRoot* software

After detection of events in *cbsim* we run these files in *acqu*. It collects all the information from the *TA2Crystal Ball* (group of detectors): (see 5.2). After detection *acqu* reconstruct the related events yielding the invariant and missing mass to identify the specific particle. These yielding events as results are given below.

5.6.1 Mass of two gamma curve

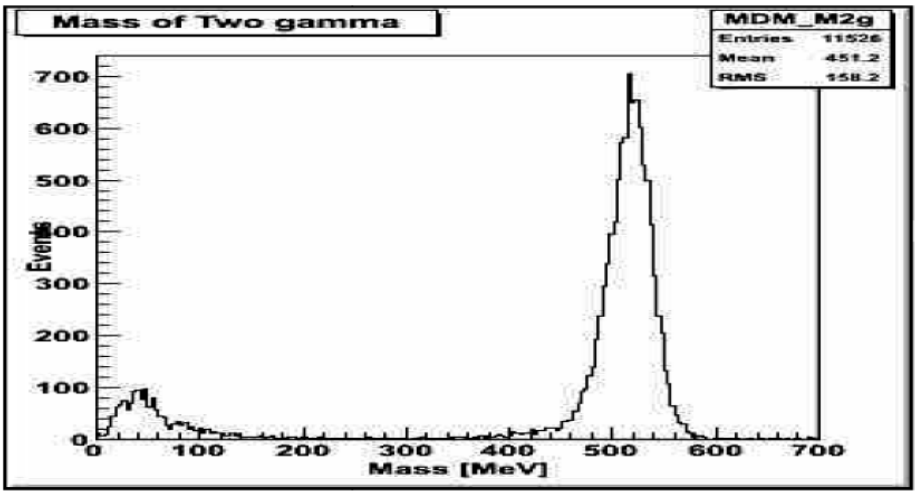

Figure 5.41: Mass of two gamma in the reaction γp→ηp → γγp

Mass of two gamma curves is drawn events versus Mass (in MeV**).** This is the result of combination of all files made in *acqu* in the energy range from 710 MeV to 1510MeV. There is peak in between 500 to 600 MeV**.** It means the peak is approximately equal to mass of *eta meson* i.e.550 MeV. Since we know the mass of *eta meson* is 550.095 MeV/c^2.In our study of photoreaction is $\gamma p \rightarrow \eta p \rightarrow \gamma\gamma p$, photon beam is incident on the liquid hydrogen target and produces *eta meson* and *proton.* The mid event ηp could not be detected by the detectors in the *Crystal Ball* and *TAPS* because the lifetime of *eta meson* is very short i.e.10^{-18}s.After decaying of *eta meson,* two *photons* were detected in *Crystal Ball and TAPS*. The detected mass of two gammas is near to the invariant mass of *eta meson* as shown in Fig. 5.42.

5.6.2 Mass of proton curve and ThetaCM curve

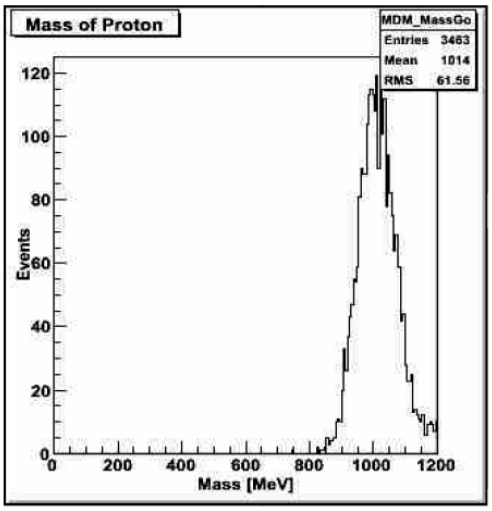

Figure 5.42: Mass of proton curve in the reaction $\gamma p \rightarrow \eta p \rightarrow \gamma\gamma p$

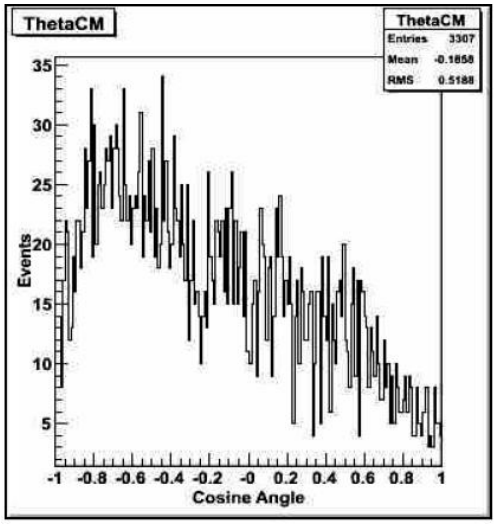

Figure 5.43: ThetaCM curve reaction $\gamma p \rightarrow \eta p \rightarrow \gamma\gamma p$

The *acqu* yields mass of proton curve, which is drawn events versus *Mass* (in MeV). This is another result of combinations of all files made in *acqu* in the energy range from 710 MeV to 1510 MeV**.** In Fig. 5.42, the peak of the curve is in between 900 to 1000 MeV. Since mass of proton is 938.27 MeV/c^2. The mass of curve from *acqu* is approximately equal to the mass of proton. It clarifies that proton was also produced in our studied reaction $\gamma p \rightarrow \eta p \rightarrow \gamma\gamma p$ and justifies the possibility of our reaction. In other words certainly our reaction has occurred. Fig. 5.43 is the ThetaCM curve

obtained from *acqu* is drawn events versus cosine angle. This cosine angle refers to the angle made by *eta meson* with the direction of incident photon beam.

5.6.3 Results obtained from TAPS and Crystal Ball

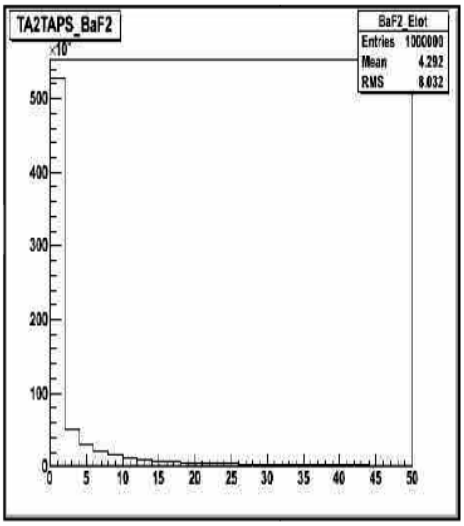

Figure 5.44: Variation of total energy of BaF_2crystals in TAPS

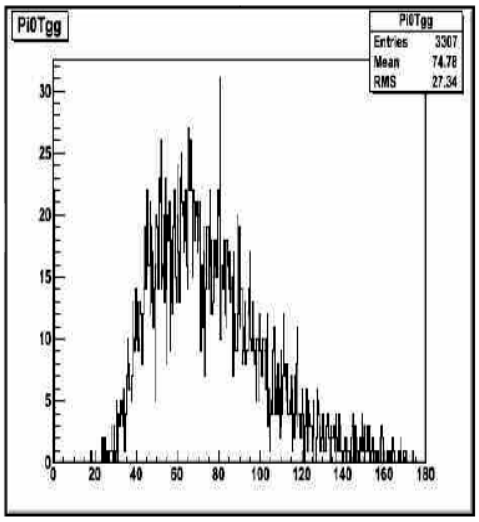

Figure 5.45: Variation of angle between two produced photon

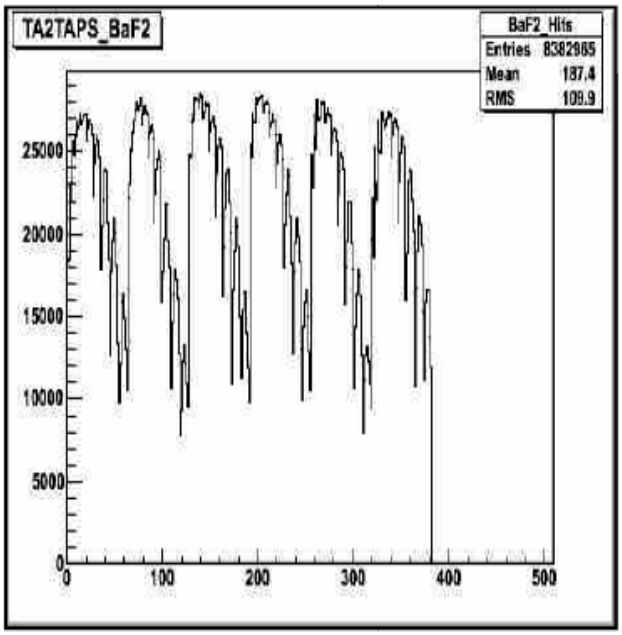

Figure 5.46: Position of elements of BaF_2 crystals in TAPS

Fig. 5.44 shows that energy measured by 384 elements of *BaF2 Crystal*. Because of having the property of high energy resolution of BaF2 detects the particle with the help of corresponding energy value. The energy is near to 500 MeV, it means mass of

eta is near to 550 MeV. It means eta meson was detected by *BaF2* crystal. Fig. 5.45 shows variation of angle between two produced photon. It shows the peak is below 90° which indicates that there is low angle variation in produced photons. Figure 5.46 shows that position of 384 elements of *BaF2 crystal in TAPS.* The result obtained from *cbsim* (Fig.5.40) software and *acqu* software (Fig. 5.46) matches almost.

5.6.4 Results related with NaI Crystal in Crystal Ball

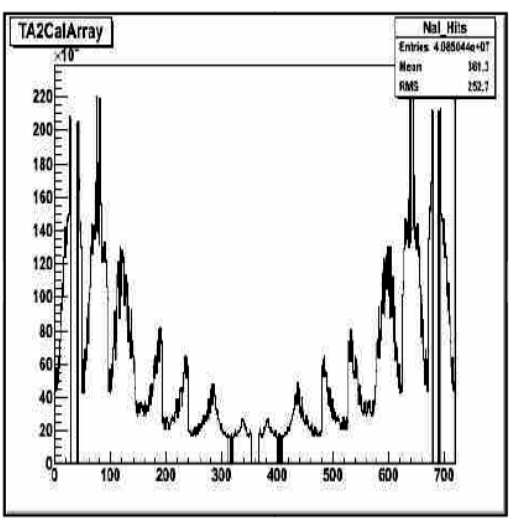

Figure 5.47: Position of elements of NaI crystal in Crystal Ball

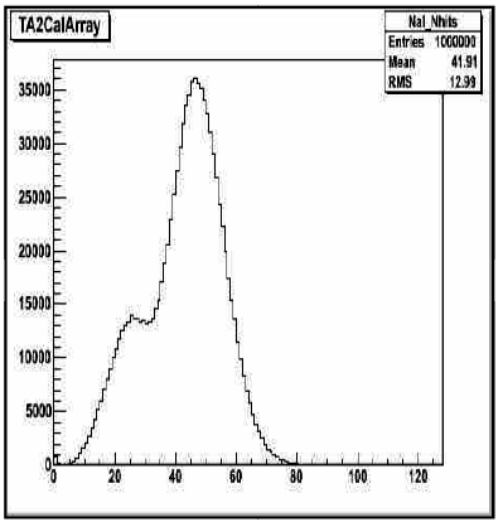

Figure 5.48: Average number of hits by the incident photon to the NaI crystal

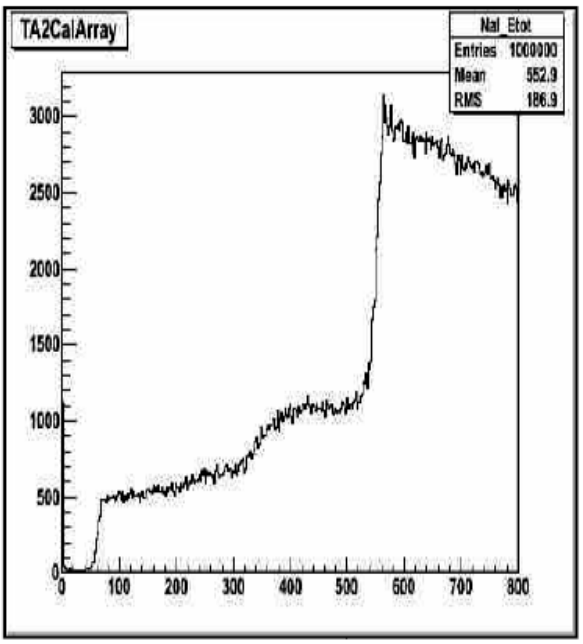

Figure 5.49: Total energy variation in the NaI crystal

Fig5.47 shows position of 720 elements of NaI crystal. Average number of hits by the incident photon to the NaI crystal is shown in Fig5.48 of Crystal Ball detector**.** In addition, the average hit is about 50. Fig 5.49 shows that the energy deposited in the NaI crystal. After incident of photon beam to the target, some energy deposition occurs in the NaI crystal**.** There is higher deposition of energy at the end and lower in the middle.

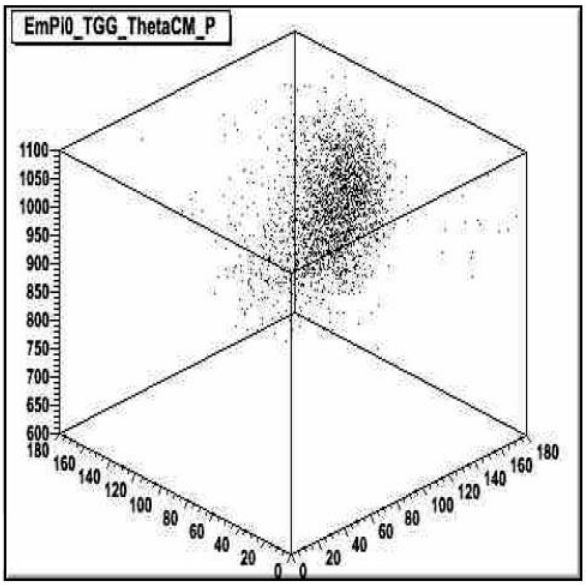

Figure 5.50: Three-dimensional figure of missing mass of pi0 (or two gamma),

Angle between twp photons and ThetaCM

This three dimensional Fig 5.50 sows that variation of ThetaCM, variation of angle between two photons and variation of missing mass of *eta meson.* Missing mass of *eta meson* (in figure missing mass of Pi0) gives mass of *proton.* Two axes in the plane shows the variation of angle *ThetaCM* which is the angle made by *eta meson* with the target and angle between two photons and in vertical axis the dark part corresponds to the missing mass of *eta meson* or mass of proton in the photoreaction $\gamma p \rightarrow \eta p \rightarrow \gamma\gamma p$. The dark part corresponds to 950 MeV, gives mass of proton in vertical axis. The dark part corresponds to the angle below 90^0 in two horizontal axis shows that there is low angle variation in angle made between two protons as well as angle made by eta meson with incident photon beam.

5.7 Comparison of results with the previous measurements

5.7.1 Comparison of position of elements of NaI crystal

We compared our results of position of elements of NaI crystal detector in *Crystal Ball* (which is virtual detector) with the experimental result obtained at MAMI-C. The result of experiment is based on the real data taken in 2007 [13].

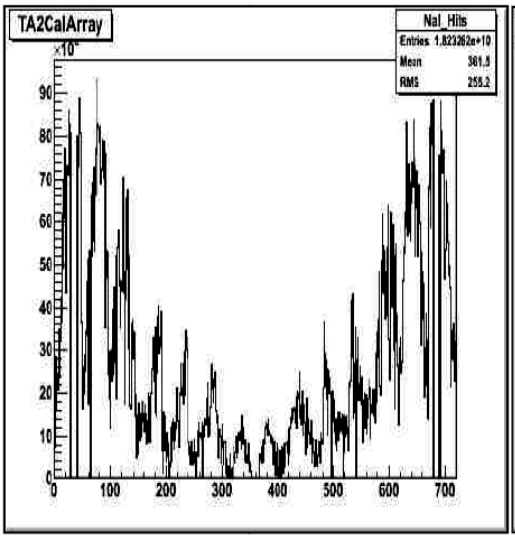

Figure 5.51: Experimental data of position of Elements of NaI crystal

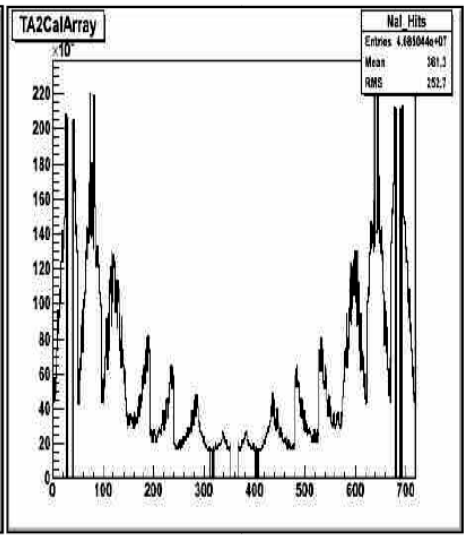

Figure 5.52: Our result of position of elements of NaI crystal obtained by Monte Carlo Simulation

By observing the histograms shown above in Fig 5.51 and Fig. 5.52, we can found that there is an approximate similarity between experimental data and result obtained by using Monte Carlo simulation**.** Both figures explain to facilitate position of elements of 720elements of *NaI crystal* in *Crystal Ball*. Both figures are quite similar. It is an interesting result, both experimental and our result matches. The events measured by NaI are helpful to measure the energy deposited due to the incident of high-energy photon to the NaI crystal.

5.7.2 Comparison of position of elements of BaF2crystal

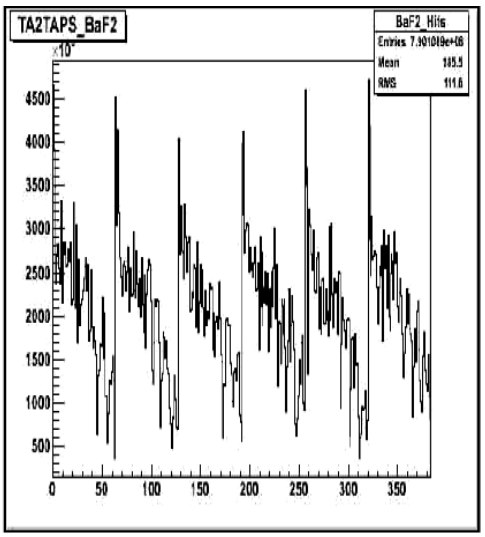

Figure 5.53: Position of elements of the 384 Elements of BaF_2 Crystals in the TAPS experimentally

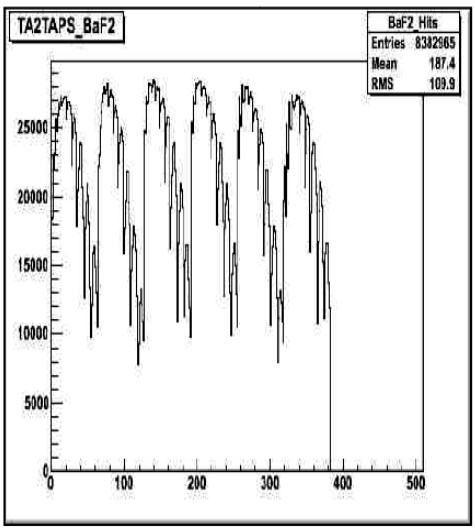

Figure 5.54: Our result of the position of elements of the 384 elements of BaF_2 crystal in virtual TAPS

Fig 5.53 and Fig 5.54 show that position of elements of 384 elements of NaI crystal in virtual TAPS detector. Both experimental result Fig. 6.50 and Monte Carlo simulation result Fig 5.54 are in quite agreement. *TAPS* was designed with the purpose to study high-energy photon beams as well as neutral mesons.

CHAPTER 6

Result Analysis

In this chapter we compare our experimental results with standard value and with other similar experiments. Our experiment was performed for incident photon over energy 702.77 MeV (threshold energy) from 710 MeV to 1510 MeV. In our target liquid hydrogen is strike by photons of these different energies. First, event was generated in *deckin* within mami_mcarlo, constructed using root, detected by *cbsim* and finally events are reconstructed with *acquRoot.*

6.1 Mass of eta meson comparision

We compared the graph of mass of *eta meson* obtained by McNicoll, Eilidh F [12] with our result obtained by using Monte Carlo Simulation. The graphs are shown below for the purpose of comparison.

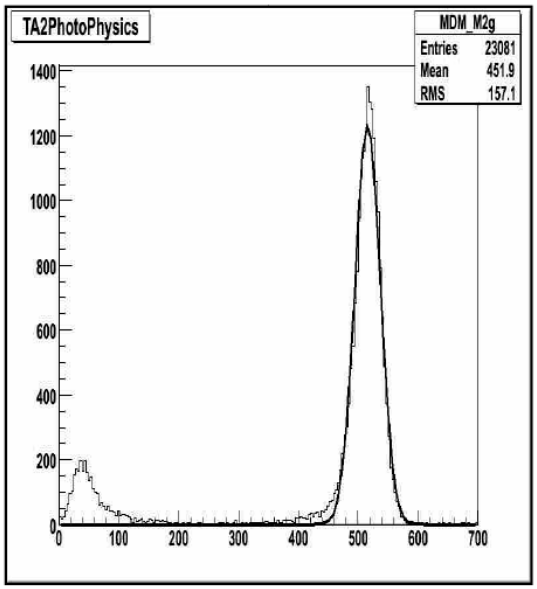

Figure 6.1: Our result of mass of eta

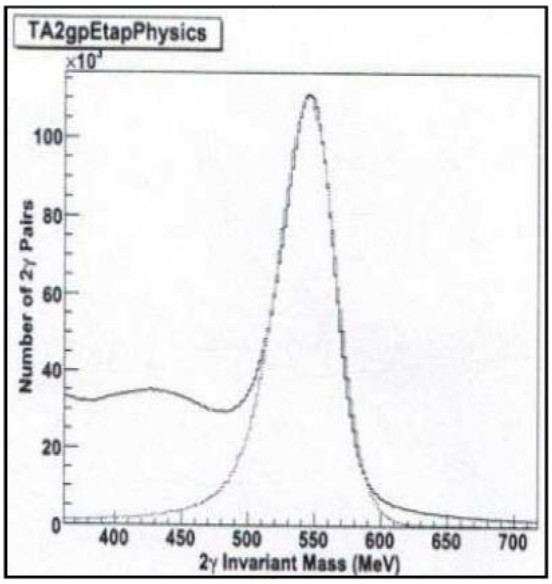

Figure 6.2: Mass of eta curve obtained by McNicoll in 2010

From these graphs, the nature of the curves found to be similar i.e. peak of the both mass of proton curves is approximately 550.095 MeV/$c^2$and our result is in good agreement with the previous result. In Fig.6.52**,** indicates our result of mass of two gamma after applying *Gaussian distribution* and Fig.6.53 is mass of of eta curve obtained by McNicoll in 2010.

6.2 Mass of proton comparison

Similarly we compared the graph of mass of proton obtained by McNicoll, Eilidh F [9] with our result. The graphs are shown below for the purpose of comparision.

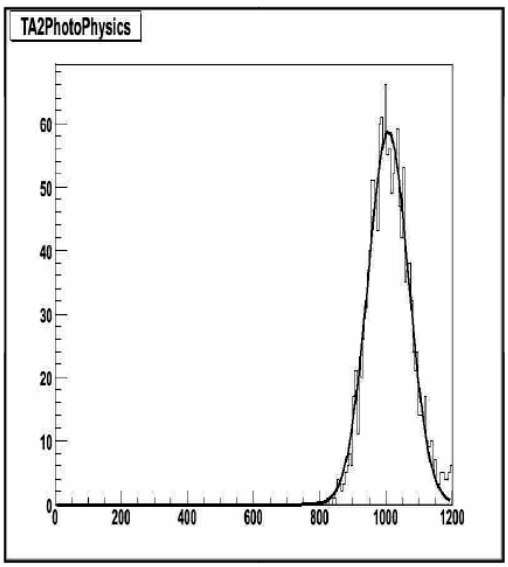

Figure 6.3: Our result of mass of proton Curve obtained by using Monte Carlo Simulation

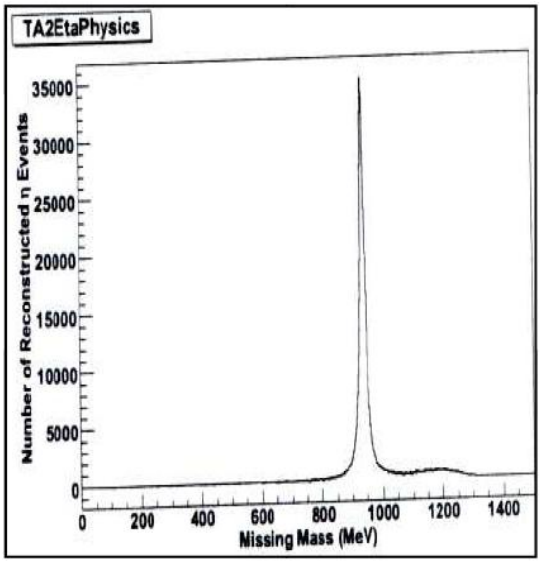

Figure 6.4: Mass of proton curve obtained by McNicoll in 2010

From these graphs, the nature of the curves found to be similar. Both curves has peak near to the mass of *proton* i.e.938.27 MeV/$c^2$and our result is in good agreement with the previous works.

6.3 Summary and Conclusions

In this dissertation, we have studied the reaction of γp→ ηp→ γγp. This reaction accomplished by using **Monte Carlo Simulation** method. In our simulation method virtual experimental set up was designed. Choosing suitable value for the energy of the photon beam, we made different *dat*files. These files were run under *mkin* software and events were generated. Important generated events in the form of histograms were generation of *photon beam*, *eta meson*, *proton*, two *photons* and *target vertex*. These generated events were detected by using *cbsim* software. In this section, we observed histograms related with identification of particles, vertex and beam. Position of elements of virtual detectors i.e. *Crystal Ball* ad *TAPS* were also detected. After that, we reconstructed events by using *acquRoot* software. From reconstruction, we studied histograms of *mass of eta meson*, *mass of proton*, *thetaCM* curves and position of elements of detectors.

From the reconstructed events invariant mass of *eta meson* and missing mass of *eta meson* or *proton mass* was found approximately 547 MeV/$c^2$and 938 MeV/c^2respectively, which were expected results. *Mass of proton* curve and *eta meson* curvewere studied by applying *Gaussian distribution*. Moreover, histograms of position of elements of NaI crystal in Crystal Ball and BaF2crystal in TAPS obtained from *cbsim* software and *acquRoot* software closely matched. At final, we compared our results with the results obtained from previous simulation as well as experimental works and both results were found similar. Our study of *eta meson* production from **Monte Carlo Simulation** will be very helpful for the determination of important features e.g. *acceptance*, *tagging efficiency*, differential and total *cross section measurements* of γp → ηp reaction.

Bibliography

[1] D. C. Tayal, Nuclear *Physics*, New Offset Printers, New Delhi (2004).

[2] H. D. Young and R. A. Freedman, *University physics*, Pearson Education (2003).

[3] R. Murugeshan and K. Shivaprakash, *Modern Physics*, S. Chand and Company Ltd. (2009).

[4] J. S. Kovacs and W. C. Lane, Fundamental Forces And Elementary Particle Classification, Michigan State University (2010).

[5] R. Oeter, *The Theory of Almost Everything: The Standard Model*, Penguin Publication (2006).

[6] G. Mann and Y. Neymaan, PhyRev.Lett**8**, 214 (1964).

[7] G. Zweig, Origin of the Quark model, CALT **68**, DOE Research and Development Report(1989).

[8] K. R. Bantawa, Photoproduction of Neutral Kaons on Deuterium, PhD Thesis, Kent State University, USA (2009).

[9] A. Jankowiak, A. Azima, S. Dusterer, J. Feldhaus, H. Schlarb and A. L. Cavalieri, EPAC, **1076**, Paris (2002).

[10] J. P. McGeorge and P. P. Martel, Eur. Phys. J.A**37,** 129 (2008).

[11] E. F. McNicoll, Eta Photoproduction Study With the Upgraded Glasgow Tagger at MAMI, PhD Thesis, University of Glasgow, Scotland (2010).

[12] J. D. Jackson, *Classical Electrodynamics*, Third Edition, John Willey and Sons, USA (1998).

[13] C. Patrignani***et al.*** (Particle Data Group), Chin. Phys. C, **40**, 100001 (2016) and 2017 update.

[14] W. B. Brudvik, Measurement of the branching ratio for eta-meson decay into a neutral pion and two photons, PhD Thesis, University of California, USA (2007)

[15] S. Homma, M. Kawaguchi and H. Miyazawa,Physical Society of Japan, **57**, 828(1998).

[16] M. Dugger,Eta (547) and Eta (958) Meson Photoproduction on the proton, PhD Thesis, Arizona State University (2001).

[17] A. Nikolov and Z. Kasachstan, Determination of the η mass from the production threshold for the $\gamma p \rightarrow \eta p$ reaction, PhD thesis, RheinischenFriedrich-Wilhelm-Universitat Bonn (2011).

[18] F. Zehr, Double pion photoproduction of the proton at threshold and in the second resonance region, PhD Thesis, University of Basel, Switzerland (2008).

[19] K. T. McDonald, Neutral pion Decay, Princeton University (1996).

[20] D. P. Watts, The Crystall Ball Program at MAMI for the Crystal Ball At MAMI Collaboration, Institute for Kern Physik, Johannes Gutenberg University, Mainz (2011).

[21] V. Bekrenev, Study of Narrow Resonance on MAMI-C, PhD Thesis, Petersburg Nuclear Physics Institute, Russia (2007).

[22] C.M. Tarbert, Coherent π^0 Photoproduction on Nuclei,University of Edinburgh, Doctor of Philosophy (2007).

[23] E. D. Bloom and C. W. Peck, Ann. Rev. Nucl. Part. Sci. **33**, 143 (1983).

[24] R. S. Kessler, R. Abegg, A. Baldisseri, A. Boudard, W. Brisco, B. Fabbro and M. Garconr, Phy Rev. Lett**70**, 892 (1993).

[25] J. Albert, Diploma Thesis, Institute for Kern Physik, Johannes Gutenberg University, Mainz (2003).

[26] D. Piparo, G. Quast and M. Zeise, *A Root Guide For Students "Diving Into ROOT"* (2005).

[27] R. Brun and F. Rademakers, *ROOT User's Guide***4.16**, CERN (2006).

[28] R. A. Arndt, W. J. Briscoe and L. Strakovsky, Analysis of Photoproduction Data, George Washington University, Washington D.C. (2002).

[29] T. Bose, Root Tutorial, Brown University, NEPPSR (2007).

Appendix A

A.1*dat*file

The file name is *newetagama_1600.dat*.

0!	Startup Seed.gamma p -> pi0 p	*Row1*
F 0 0 0 F !	Select (T/F)?,hid_cs, hid_ang, cm_var, err_check (T/F)?	*Row 2*
1 !	Beam Particle GEANT id	*Row 3*
1.7350.1 !	Beam momentum, dP/P (std. dev., %)	*Row 4*
.2 .2 !	Beam Sigma(x), Sigma(y) (std. dev., cm)	*Row 5*
0.5 0.5 !	Beam Sigma_ThX, Sigma_ThY (std. dev., mrad)	*Row 6*
14 5.0 !	Target Particle GEANT id, Target Length (cm)	*Row7*
FALSE !	Use a distribution function?	*Row8*
17 TRUE 0 !	ram id# eta *1* particle	*Row9*
14 FALSE 0 !	Part. id#, decay logical # proton 2 particle	*Row10*
-1 !	Terminate list of decay products	*Row11*
FALSE 0.0 180.0 0.0 360.0 !Limit CM angular range?		*Row12*
1 FALSE 0 !	photon3 particle, decay product of eta	*Row13*
1 FALSE 0 !	photon4 particle, decay product of eta	*Row14*
-1 !	Terminate list of decay products	*Row15*
FALSE 0.0 180.0 0.0 360.0 !Limit CM angular range?		*Row16*

Explanation:.

Row 3: **1**! Beam particle GEANT id represents striking particle is gamma

Row 4: **1 .735** represents the energy of striking particle gamma is 735 MeV

Row 7: **14** represents GEANT id of target i.e. liquid hydrogen, 5 target length between striker and target

Row 9: **17 TRUE**: after striking *eta* is produced and TRUE means it further breaks

Row 10: **14 FALSE** means proton is produced and FALSE means it does not break

So in first case after striking liquid hydrogen by gamma eta and proton are produced.

$$\gamma p \rightarrow \eta p$$

Row 13: 1 FALSE means *eta* breaks into 1st photon and photon does not break further

Row 14 : 1 FALSE means eta breaks into 2nd photon and photon does not break further so our final reaction becomes in the form of

$$\gamma p \rightarrow \eta p \rightarrow \gamma\gamma p$$

In above file **1.735** represents energy of incident gamma ray is 735 MeV. 1! Beam particle **GEANT id** represents gamma strikes liquid hydrogen target is symbolized as GEANT id 14**.** After striking by *gamma eta particle and proton* produced, this is represented as 17 TRUE for eta and 14 FALSE for proton. Symbol TRUE means eta particle is further breaks and FALSE means proton does not break. Eta breaks into two gammas in succession which is represented as 1 FALSE.

Appendix B

B.1*mkin* file

if ($# != 1) then

echo "ERROR: Must input either nothing (which runs all targets and \energies), 'eg' which uses a specific Energy Channel and \energy range."

echo " 'mkin_cb.sh 900'"

echo " or 'mkin_cb.sh ....MeV'"

exit 0

endif

setinc = 711

seteg = $1

set end = 1600

if($eg> $end) then

echo "ERROR : eg>end"

exit 0

endif

if($end > 1600) then

echo "Error : end > 1600 MeV"

exit 0

endif

while($eg<= $end)

setmkin_file=/home/devshree/mami_mcarlo/results_deckin/deckin_newetagama_$eg.hbook

if(! -e $mkin_file) then

echo "Input files $mkin_filedoesnot exit . skkipping ....."

seteg = `expr $eg + $inc`

continue

endif

setcb_file = /home/devshree/mami_mcarlo/results_cbsim/

new_devshg.$eg.hbook

setroot_file = /home/devshree/mami_mcarlo/results_cbsim/new_devshrg.$eg.root

setenv FFCARDS
/home/devshree/mami_mcarlo/jb_ffcards_files/gamaeta.ffcards

setenv NTTITLE $cb_file

setenv INPUTFILE $mkin_file

setenv OUTPUTFILE $cb_file

cd /home/devsh/mami_mcarlo/cbsim

./crystalball

h2root $cb_file $root_file

wait

seteg = `expr $eg + $inc`

end

end

exit

Inside mkin file bold letter places and italic letter places represent our

correction.

Appendix C

C.1 Gaussian distribution

One of the most important probability distribution, which has wider applications, is the Gaussian distribution. This distribution also called Normal distribution. In this distribution the variation in x has following distribution of the form

$$P(x) = 1/\sigma\sqrt{2n}.e^{-1/2(x-\mu)/\sigma)2}dx, \quad -\infty \leq x \leq \infty$$

$p(x)=f(x)dx$ when

$$f(x) = 1/\sigma\sqrt{2n}.e^{-1/2(x-\mu)/\sigma)2}$$

(a)

$y=f(x)$ is called normal probability curve.

When $z=(x-\mu)/\sigma$, $p(z)= 1/\sqrt{2n}.e^{-z2/2}dz$

(b)

z is called standardized normal variate.

C.2 Chief Features of Normal distribution

1. The Curve is bell shaped and symmetrical about limit x=μ
2. Mean, Median and Mode of the distribution coincide.
3. As x increases numerically, f(x) decreases rapidly. The maximum probability is at point x=μ and is given by [P(x)max] = 1/ σ√2π

Nature of Curve for Normal Distribution

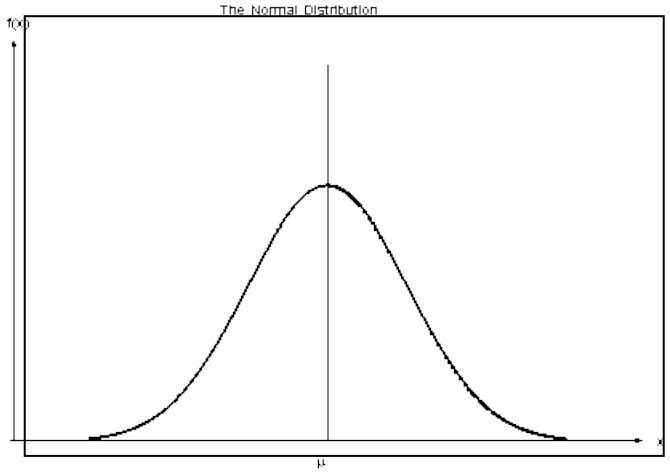

Figure: Normal distribution Curve, Source: Wikipedia**s**